IOWA STATE UNIVERSITY
Digital Repository

2012

Analytical solution of an advective zone model

Greta Fayette Schmalle
Iowa State University

Follow this and additional works at: https://lib.dr.iastate.edu/etd

Part of the Civil Engineering Commons, and the Environmental Engineering Commons

Analytical solution of an advective zone model

by

Greta Fayette Schmalle

A thesis submitted to the graduate faculty

in partial fulfillment of the requirements for the degree of

MASTER OF SCIENCE

Major: Civil Engineering (Environmental Engineering)

Program of Study Committee:
Chris Rehmann, Major Professor
Roy Gu
Kristie Franz

Iowa State University

Ames, Iowa

2012

This thesis is dedicated to my grandfather, Robert. E. Dietz, who has been
a great role model to an aspiring engineer.

TABLE OF CONTENTS

ACKNOWLEDGMENTS

NOTATION LIST

A = cross-sectional area

B = channel width

C = concentration

$\overline{C}$ = mean concentration

C' = deviation from mean concentration

C^* = dimensionless concentration

C_0 = initial concentration

C_1 = concentration in the flowing zone (Reichert and Wanner, 1991)

C_2 = concentration in the stagnant zone (Reichert and Wanner, 1991)

C_1^* = dimensionless concentration in the flowing zone

C_2^* = dimensionless concentration in the stagnant zone

C_d = concentration in the dead zone (dead zone model)

C_p = peak concentration

C_m = concentration in the main channel (dead zone model)

c_f = alternative dimensionless dispersion coefficient (Fischer, 1975)

D = diffusion coefficient

D_x = mixing coefficient in x direction

D_y = mixing coefficient in y direction

F_{nx} = n^{th} spatial moment in flowing zone

g = numerator of the spatial skewness coefficient, γ

g_t = numerator of the temporal skewness coefficient, γ

g_{tm} = numerator of the measured temporal skewness coefficient, γ

h = channel depth

I = area under the dimensionless time-concentration curve

K = dispersion coefficient

K_x = longitudinal dispersion coefficient

k_α = longitudinal curvilinear dispersion coefficient

k_β = transverse curvilinear dispersion coefficient

L = length

L_G = distance to Gaussian zone

L_t = transverse length

L_x = advective length

M = mass of tracer

$\dot{M}$ = mass transport

M_0 = initial mass of tracer injected

M_{0f} = mass in the flowing zone

M_{0s} = mass in the stagnant zone

M_n = nth moment

M_{nx} = n^{th} spatial moment

M_{nt} = n^{th} temporal moment

m_α = metric longitudinal curvilinear coefficient

m_β = metric transverse curvilinear coefficient

Q = discharge

q = cumulative discharge

q_e = transfer coefficient

S_{nx} = n^{th} spatial moment in stagnant zone

T_c = scaling parameter (Day and Wood, 1976)

t_p = time to peak

t = time

t' = dimensionless time

t_a = time of advection

t_{eq} = time to equilibrium

U = velocity in the x-direction

$\overline{U}$ = mean velocity in the x-direction

U' = deviation from mean velocity in x-direction

u^* = shear velocity

V_s = volume of solute

V = depth-averaged transverse velocity

v_α = depth-averaged longitudinal curvilinear velocity

v_β = depth-averaged transverse curvilinear velocity

x = longitudinal coordinate

x' = dimensionless distance

y = transverse coordinate

z = vertical coordinate

α = ratio of channel occupied by stagnant zone to main channel

α^* = coefficient for advective length

α_c = curvilinear coordinate for the longitudinal distance

α_d = mass exchange coefficient between main channel and dead zone

α_x = dimensionless dispersion coefficient

β = normalized transfer coefficient

β_c = curvilinear coordinate for the transverse distance

β_d = ratio of area in dead zone to area in main channel

γ = skewness coefficient

γ_t = temporal skewness coefficient

γ_x = temporal skewness coefficient

γ_p = dimensionless width of pulse (Reichert and Wanner, 1991)

Δx = initial width of pulse (Reichert and Wanner, 1991)

$\delta(x)$ = Dirac delta function

ε_y = lateral mixing coefficient

θ = dimensionless transverse mixing coefficient

μ = center of mass

μ_t = temporal center of mass

μ_{tm} = measured temporal center of mass

μ_x = spatial center of mass

μ_f = spatial center of mass in flowing zone

μ_s = spatial center of mass in stagnant zone

σ_0 = initial spread of pulse

σ^2 = variance

σ_t^2 = temporal variance

σ_{tm}^2 = measured temporal variance

σ_x^2 = spatial variance

σ_f^2 = spatial variance in flowing zone

σ_s^2 = spatial variance

τ = time in transformed coordinate system

ξ = Lagrangian coordinate for flow direction

ψ = dimensionless width of the pulse

LIST OF FIGURES

LIST OF TABLES

ABSTRACT

An analytical solution of a model of contaminant transport in the advective zone of rivers was derived and tested. Although the standard one-dimensional model of transport cannot be applied near the contaminant source, the transport model proposed by Reichert and Wanner (1991), which requires only one more parameter to be specified, applies over much of the advective zone. The model was solved with Laplace transforms for the case of a Gaussian pulse injected into the center of the channel and verified through an analysis of the spatial and temporal moments. The moment analysis demonstrated the importance of carefully evaluating the integrals in the analytical solution. To help in applying the model to field measurements, the effects of the model parameters were investigated and a procedure for determining the parameters from measurements was devised. The model was applied to measurements in the advective zone of a mountain stream. Predictions from the Reichert and Wanner model fit the measurements—especially the peak concentration and arrival time— better than predictions from the one-dimensional model.

CHAPTER 1: INTRODUCTION

Significance

Despite the limitations in describing tracer response curves in real channels, solutions of the one-dimensional advection-dispersion equation, such as the one developed by Taylor, are still used to compute contaminant transport. However, because the one-dimensional approach applies only after a balance between longitudinal advection and transverse dispersion has been reached, other models must be used to compute concentrations in the near-field, or the 'advective zone'. In many rivers, this length of the advective zone is several hundred kilometers long. Reichert and Wanner (1991) developed and evaluated a model that consists of a flowing zone and a stagnant zone; instead of the single parameter (i.e., the dispersion coefficient) in the one-dimensional model, it involves two parameters: the fraction of the channel occupied by the stagnant zone, α, and a transfer coefficient, q_e. However, because the authors did not give details on how they computed concentrations with their model, its application for those who model dispersion processes within the advective zone is limited.

Objectives

This work aims to (i) obtain and verify an analytical solution of the Reichert and Wanner (1991) advective zone model; (ii) understand the behavior of the model by analyzing spatial and temporal moments; and (iii) apply the analytical solution to field data measured within the advective zone.

The analytical solution is obtained through the application of an iterative Laplace transform given by Sneddon (1972). This process has been applied successfully by De Smedt et al. (2005) in the derivation of an analytical solution of the dead zone model. The behavior of the model is analyzed with the analytical expressions for the spatial and temporal moments. These expressions were obtained through solving a set of ordinary differential equations (for the spatial case) and through Laplace transforms (for the temporal case). These solutions also serve as verification of the analytical solution. Finally, the analytical solution to the Reichert and Wanner model is applied to field data measured by Day (1975) in the advective zone of a mountainous stream. The predicted results from this analysis are compared with the measured concentration curves and the predicted results from Taylor's dispersion model.

Organization

In this thesis, a background of mechanisms controlling dispersion, as well as a review of existing work in dispersion modeling is presented in Chapter 2. Chapter 3 addresses the development of the analytical solution, the methods for verifying the solution, and the methods for applying the solution to measured data. In Chapter 4, the predicted temporal and spatial concentration curves, as well as the moments derived from the integration of the predicted curves, are presented and discussed. A summary of this work, as well as recommendations for future work, is given in Chapter 5.

CHAPTER 2: BACKGROUND AND LITERATURE REVIEW

Introduction

Contaminant transport in natural channels is a critical issue in the field of environmental engineering, and as a result, the processes controlling mixing and movement in channels have been extensively studied so that contaminant transport can be modeled effectively and accurately. Longitudinal dispersion describes the spreading of contaminants or tracers along the flow direction. It is a necessary process to include when estimating the arrival time, concentration, and spread of a contaminant. The methods used to model longitudinal dispersion vary in their assumptions regarding flow processes, mathematical complexity, and applicability with respect to channel location. This chapter outlines the development and appropriate application of various models for predicting concentrations of contaminants; additionally, it addresses the areas where additional research and development would improve current longitudinal dispersion models.

Mechanisms Controlling Longitudinal Dispersion

Velocity gradients cause longitudinal dispersion. Transverse gradients of velocity arise because velocities are zero at the channel boundaries—i.e., banks for natural channels. Tracer particles move across the channel cross section because of motions in eddies. When travelling, they experience different velocities and some tracer parcels move faster than others. As a result, the tracer cloud spreads along the channel as it moves downstream. The contributions of vertical velocity shear and vertical diffusion are often ignored when analyzing longitudinal mixing because natural channels have much greater widths than

depths and the tracer becomes well-mixed over the channel depth shortly after injection. The

contribution of longitudinal diffusion can also be ignored because it is small compared to

effects of transverse velocity shear. Therefore, longitudinal dispersion depends mainly on

transverse velocity shear and transverse diffusion. Over time, these terms eventually reach

equilibrium, and the variance of the tracer distribution grows linearly, as shown by the

analysis of Taylor (1953). This balance only holds true if other mechanisms do not

significantly contribute to longitudinal dispersion. This is not always the case, especially in

natural channels.

Natural channels include additional mechanisms that influence mixing, specifically

exchange between the main channel and dead zones. A dead zone is a region of irregular

flow compared to the flow regime in the main channel. Irregularities can be caused by

eddying or stagnant flow. These irregularities increase dispersion in the channel (Fischer et

al., 1979). Increased dispersion lengthens the time it takes for the transverse velocity shear

and transverse diffusion to reach equilibrium (Valentine and Wood, 1977). Until equilibrium

is reached, the tracer distribution will exhibit a skew. This skew is observed in field studies in

the form of a long tail in tracer response curves (Nordin and Sabol, 1974; Day, 1975). The

persisting skew complicates the analysis of field results, and as a result, some researchers

have chosen to ignore it. Fischer (1968) ignored the tail of the recorded response curves and

found that the non-tail portion of the curve agreed well with Taylor's analysis. In cases

where researchers choose not to ignore the tail, alternative models were used to describe

longitudinal dispersion (Nordin and Troutman, 1980; Legrand-Marcq and Laudelout, 1985;

Davis et al., 2000). The most common alternative model, which will be discussed later, is

the dead zone model.

Taylor's Analysis

The conventional approach used to describe shear dispersion in natural channels is based on Taylor's analysis of diffusion (Taylor 1953, 1954). Taylor's analysis shows that over time the longitudinal advection and transverse mixing reach equilibrium. Once equilibrium is reached, diffusion can be modeled as a Fickian process, in which the variance of the tracer concentration distribution increases linearly with time. Taylor applied his analysis to describe longitudinal mixing of a contaminant in laminar and turbulent flow through a pipe (Taylor, 1953 and Taylor, 1954, respectively). Elder (1959) extended this analysis to include the effects of vertical shear, and Fischer (1966) used it to compute longitudinal dispersion in open channels. Taylor's theory, when applied to pipe and open channel flow, has been verified by several laboratory studies (Fischer, 1966; Sayre, 1968; Sayre and Chang, 1968). Additionally, Aris (1956) confirmed Taylor's results through his independent analysis using the method of moments.

In order to understand the major assumption behind Taylor's analysis and the conditions under which the analysis does not apply, the one-dimensional advection-dispersion equation (1-D ADE) is derived following the analysis in Fischer et al. (1979, section 4.1.4). This analysis starts with the two-dimensional advection-diffusion equation for concentration C given by

$$\frac{\partial C}{\partial t} + U \frac{\partial C}{\partial x} = D \left[\frac{\partial^2 C}{\partial x^2} + \frac{\partial^2 C}{\partial y^2} \right] \tag{1}$$

where U is the velocity in the x-direction and D is the molecular diffusivity. Eq. 1 assumes that flow is in the x-direction and that the velocity components in the transverse and vertical directions are zero. Additionally, this equation assumes that the concentration is uniform

over the depth. The velocity and concentration can be written as the sum of the cross-sectional average and the deviation from the average:

$$U(x, y) = \bar{U} + U'(x, y) \tag{2}$$

$$C(x, y, t) = \bar{C} + C'(x, y, t) \tag{3}$$

where

$$\bar{U} = \frac{1}{B} \int_0^B U \, dy \tag{4}$$

and

$$\bar{C} = \frac{1}{B} \int_0^B C \, dy \tag{5}$$

and B is the width of the channel. The transport equation can be re-written as

$$\frac{\partial}{\partial t}(\bar{C} + C') + (\bar{U} + U')\frac{\partial}{\partial x}(\bar{C} + C') = D\left[\frac{\partial^2}{\partial x^2}(\bar{C} + C') + \frac{\partial^2 C'}{\partial y^2}\right] \tag{6}$$

To simplify the expression further, the coordinate system can be defined in Lagrangian terms, i.e., moving with the flow, so that

$$\xi = x - \bar{U}t \tag{7}$$

$$\tau = t \tag{8}$$

Changing the coordinate system, Eq. 6 becomes

$$\frac{\partial}{\partial \tau}(\bar{C} + C') + U'\frac{\partial}{\partial \xi}(\bar{C} + C') = D\left[\frac{\partial^2}{\partial \xi^2}(\bar{C} + C') + \frac{\partial^2 C'}{\partial y^2}\right] \tag{9}$$

As mentioned in the previous section, diffusion in the flow direction ξ is very small compared to the spreading caused by the shear, and as a result, the diffusive term in ξ can be eliminated. This reduces Eq. 9 to

$$\frac{\partial}{\partial \tau}(\bar{C} + C') + U'\frac{\partial}{\partial \xi}(\bar{C} + C') = D\frac{\partial^2 C'}{\partial y^2} \tag{10}$$

Eq. 10 cannot be solved using standard methods because U' varies with y. However, Taylor argued that after a sufficient time, a balance between longitudinal advection and transverse dispersion is reached. This reduces Eq. 10 to:

$$U' \frac{\partial}{\partial \xi} \bar{C} = D \frac{\partial^2 C'}{\partial y^2}.$$ (11)

Integrating Eq. 11 twice gives

$$C'(y) = \frac{1}{D} \frac{\partial \bar{C}}{\partial x} \int_0^y \int_0^{y_1} U'(y_2) dy_2 \, dy_1 + C'(0)$$ (12)

Given an expression for the concentration deviation, the mass transport, $\dot{M}$, is be defined to be

$$\dot{M} = \int_0^B U'C'dy$$

$$= \frac{1}{D} \frac{\partial \bar{C}}{\partial x} \int_0^B U'(y) \int_0^y \int_0^{y_1} U'(y_2) dy_2 dy_1 dy + \int_0^B U'(y)C'(0)dy$$ (13)

The term $\int_0^B U'(y)C'(0)dy = 0$ because $\int_0^B U'dy = 0$. Because $\dot{M}$ is proportional to the longitudinal concentration gradient, it can be expressed in the form of Fick's law:

$$\dot{M} = -KB \frac{\partial \bar{C}}{\partial x}$$ (14)

where the dispersion coefficient, K, is

$$K = -\frac{1}{DB} \int_0^B U'(y) \int_0^y \int_0^{y_1} U'(y_2) dy_2 \, dy_1 dy$$ (15)

Averaging Eq. 10 and using Eq. 13-15 gives

$$\frac{\partial \bar{C}}{\partial \tau} = \overline{-U' \frac{\partial C'}{\partial \xi}} = -\frac{\partial}{\partial \xi} (\overline{U'C'}) = -\frac{\partial}{\partial \xi} \left(\frac{\dot{M}}{B} \right) = \frac{\partial}{\partial \xi} \left(K \frac{\partial \bar{C}}{\partial \xi} \right)$$ (16)

Writing Eq. 16 in terms of the fixed coordinate system, the 1-D ADE is finally derived:

$$\frac{\partial \bar{C}}{\partial t} + \bar{U} \frac{\partial \bar{C}}{\partial x} = K \frac{\partial^2 \bar{C}}{\partial x^2}$$ (17)

For an initial spike injection, there are three consequences of Eq. 17: (1) the variance of the mean dye concentration will increase linearly with time, (2) the skewness will decay at a rate of $x^{-1/2}$, and (3) the concentration distribution will eventually become Gaussian (Nordin and Troutman, 1980; Rutherford, 1994). These conditions apply only after all assumptions from Taylor's analysis are met—specifically, that sufficient time has passed to establish equilibrium between longitudinal advection and transverse diffusion; once this has occurred, the flow is considered to be in the 'equilibrium zone'. The portion of the channel preceding this equilibrium zone is known as the advective zone. For stationary turbulent flow, the advective zone is defined as the distance it takes a tracer particle to sample the entire flow field. As predicted by Eq. 17, the skewness will decay until the profile is Gaussian; when this occurs, the tracer is considered to be in the 'Gaussian zone' (Rutherford, 1994).

Solutions to the 1-D ADE

The 1-D ADE (Eq. 17) is a partial differential equation (PDE) which can be analyzed through a variety of techniques, including a moment analysis, numerical analysis, or analytical techniques. The method used depends on several factors including existing solutions available, resources allotted, and precision required. There are several analytical solutions to the 1-D ADE for a variety of initial and boundary conditions. The solution to Eq. 17 for an instantaneous point source injected at $t = 0$ and at location $x = 0$ is

$$\bar{C}(x,t) = \frac{M}{A\sqrt{4\pi Kt}} \exp\left[-\frac{(x-Ut)^2}{4Kt}\right] \tag{18}$$

where M is the mass of the tracer and A is the cross-sectional area of the channel. Eq. 18 predicts the spatial concentration distribution for given time after injection. In practice, it is very difficult to measure the spatial distribution of a tracer cloud; alternatively, the tracer

distribution is measured temporally at fixed locations downstream from injection. Through the frozen cloud approximation, a method used to re-route spatial distributions, measurements in time can be transformed to estimate the spatial distribution of the tracer (Rutherford 1994).

When an analytical solution is not available, the moments of the tracer distribution are useful in analyzing longitudinal dispersion. The methods used to derive moments are mathematically less complex than deriving a full analytical solution or programming a numerical solution; as a result, the moments are typically computed before numerical or analytical solutions are derived. This makes the moments a valuable check in the verification of a new solution. A drawback to the moment analysis is that concentration as a function of time or space cannot be derived.

Moments are simpler to consider because they arise from integrals of the concentration in either space or time. The nth moment of a spatial tracer distribution is defined as

$$M_n(t) = \int_{-\infty}^{\infty} x^n C(x,t) dx \tag{19}$$

A similar equation is used to compute the temporal moments. The moments describe different aspects of the tracer distribution as it advances downstream. The zeroth moment, M_0, is related to the mass M of the tracer distribution. The first and second moments, M_1 and M_2, characterize the location and spread of the distribution; the center of mass, μ, is defined as

$$\mu = \frac{M_1}{M_0} \tag{20}$$

and the variance, σ^2, is defined as

$$\sigma^2 = \frac{M_2}{M_0} - \mu^2 \tag{21}$$

The third moment, M_3, characterizes the skew, γ, given by

$$\gamma = \frac{\dfrac{M_3}{M_0} - 3\mu\sigma^2 - \mu^3}{\sigma^3} \tag{22}$$

Numerical models are often used in addition to a moment analysis because they can predict a theoretical concentration distribution with respect to time or space. Additionally, coefficients and channel parameters are able to vary to reflect changing conditions. PDEs can be solved numerically with various finite-difference methods. These methods range in their mathematical complexity and accuracy. With advances in computer technology, there is less of a disadvantage in using an advanced method; as a result, these methods are used over simpler, less precise methods. Despite this, there are still disadvantages to using a numerical method. Primarily, numerical models are not a solution to a PDE—only an approximation. All numerical solutions will have some degree of error. Error is reduced by increasing the number of time steps in the numerical computation or choosing a more rigorous numerical method; however, these both increase the computational time and required memory to run the program. Regardless, some portion of the error will inherently be due to numerical dispersion (dispersion created by numerical calculation, not through mixing mechanisms).

It is common that a new analytical model is developed when there is not a current model available to describe the conditions of interest and the user wishes to avoid the error characteristic of numerical models (De Smedt, 2006).

Estimating the Advective Length

The solutions to Eq. 17 hold only after the tracer has left the advective zone, L_x. This distance must be calculated before applying Taylor's analysis to ensure that Eq. 17 is not misused. If the channel is wider than it is deep, the distance it takes for tracer to mix across a channel is the length of the advective zone. This distance, L_x, is predicted by

$$L_x = \alpha^* \frac{\bar{U} L_t^2}{\varepsilon_y} \tag{23}$$

where α^* is a coefficient, L_t is the transverse length scale, and ε_y is the transverse (or lateral) dispersion coefficient. Rutherford (1994) defines L_t as the distance from the point of maximum velocity to the farthest bank. Therefore, it is approximately half of the width for a symmetric, straight channel. Values for α^* have been estimated by several researchers based upon results from numerical and laboratory flume experiments (Fischer, 1967; Fischer, 1968; Sayre, 1968; Fischer 1973; Chatwin, 1972; Tsai and Holley, 1978), and for smooth channels it ranges from 0.3 and 0.6 depending on the location of tracer injection. In studies with channel and bed irregularities, α^* is larger. Denton (1990) conducted a study in rough beds and estimated α^*=1.4. The sets of experiments conducted by Valentine (1978) and Valentine and Wood (1979b) in dead zones estimated α^* to range from 1.6 to >10.

Researchers have also attempted to quantify the distance to the Gaussian zone, L_G. Based on experimental results reported by Fischer et al (1979), Denton (1990), Sayre (1968), Liu and Cheng (1980), L_G has been estimated to fall within the range

$$2.5 L_x < L_G < 50 L_x \tag{24}$$

This distance is not of great importance because experimental concentration profiles

measured in natural channels do not become completely Gaussian (Nordin and Sabol, 1974;

Schmid, 2002).

Estimating the Mean Velocity and Longitudinal Dispersion Coefficient

Eq. 17 assumes that the mean velocity, $\bar{U}$, and dispersion coefficient K are constant.

When analyzing the longitudinal dispersion, K in Eq. 17 is equal to the longitudinal

dispersion coefficient, K_x. The mean velocity, defined in Eq. 2, is typically obtained from

field measurements across the channel cross-section at several points along the channels

length. If extensive field data are not available, it can be estimated by

$$\bar{U} = \frac{Q}{A} \tag{25}$$

where Q is the flow rate. Numerous field studies have been conducted to measure the

dispersion coefficient, K, for various channels and rivers (Valentine, 1978; Fischer, 1968).

However, in the case where measured results are not available for the channel or river of

interest, empirical equations have been derived to calculate K_x. Fischer (1967) modified Eq.

15 into the semi-empirical form to calculate K_x for natural channels:

$$K_x = -\frac{1}{A} \int_0^B h(y_3) u'(y_3) \left\{ \int_0^{y_3} \frac{1}{h(y_2)\varepsilon_y(y_2)} \left(\int_0^{y_2} h(y_1) u'(y_1) \, dy_1 \right) dy_2 \right\} dy_3 \tag{26}$$

where depth $h(y)$ is the depth, written as a function of the transverse location, y, and ε_y is the

dimensionless transverse mixing coefficient. Rutherford (1994) expressed the transverse

mixing coefficient as

$$\varepsilon_y = \theta u^* h \tag{27}$$

where $u*$ is the shear velocity and θ is a dimensionless transverse mixing coefficient. Holley and Jirka (1986) estimated θ to range from 0.2 and 2.0 based on their review of several flume and field experiments; larger values of θ are expected where there is more transverse mixing. Fischer (1973) used results from dispersion experiments and the relationship given in Eq. 27 to reduce Eq. 26 to:

$$K_x = \alpha_x \frac{\bar{U}^2 B^2}{\varepsilon_y} \tag{28}$$

where α_x is dimensionless dispersion coefficient. From Rutherford (1994), the range of α_x is

$$0.001 < \alpha_x < 0.016. \tag{29}$$

Eq. 26 can also be written as (Fischer, 1975):

$$K_x = c_f \frac{\bar{U}^2 B^2}{u^* h} \tag{30}$$

where c_f is a dimensionless longitudinal dispersion coefficient. Fischer (1975) determined $c_f \approx 0.011$ based on experimental results. Seo and Cheong (1998) compared the available theoretical and empirical equations for the dispersion coefficient and concluded that Fischer's (1975) empirical equation predicts measured dispersion coefficients fairly well; however, for large river widths it will overestimate K appreciably. In a later study Seo and Cheong (2001) investigated several methods for determining the model parameters for the dead zone model and found that predictions from the model with parameters estimated with the moment matching method resulted in the best fit to measured field data.

There is some degree of uncertainty associated with any value of $\bar{U}$ and K, whether it is directly measured or empirically calculated. A more precise estimate can be obtained from field testing, but the traditional tracer experiment is costly and time-consuming. Carr and Rehmann (2007) introduced an alternative method that uses acoustic Doppler current

profilers (ADCP) to estimate K. This method uses ADCP transects measured and made available by the USGS. Estimated values of K from the ADCP method have been compared to values obtained through tracer studies, and the ADCP method can predict K as well, but in most cases, better than empirical formulas.

Alternative Models

The 1-D ADE is the conventional model used to describe longitudinal dispersion in a channel; however, there are several cases where this equation is not appropriate. As a result, alternative longitudinal dispersion models have been created. Examples of where alternative models are preferred over the 1-D ADE include (1) cases where resources are not available, (2) channels with dead zones, and (3) flow in the advective zone. These alternative models vary in their complexity, accuracy, necessary input data, and application. The best model will depend on the location of interest, conditions in the channel, and the resources available.

Empirical Models

Empirical equations are useful to those who need to calculate transport processes in natural channels but do not have the data, time or computational power to use numerical or analytical solutions. This is the case for when calculations must be done immediately (e.g., in response to a contaminant spill) or the user is dealing with a very large dataset and a simplified method is preferred. Day and Wood (1976) formulated an empirical equation to predict the peak concentration, C_p, based upon the geometry of a typical response curve:

$$C_p = C_0 V_s / T_c IQ \tag{31}$$

where C_0 is the initial concentration of the solute, V_s is the volume of the solute, T_c is a

scaling parameter that describes the spread of a tracer distribution, I is the area under the

dimensionless time-concentration curve (approximately 1.12), and Q is the flow rate. T_c can

be estimated by the following empirical equation:

$$T_c \overline{U} / B = 0.24 + 0.24 x / B \tag{32}$$

where x is the longitudinal distance. Eq. 31 and 32 were derived from a regression analysis of

results recorded by Day (1975) for 702 concentration curves measured in five reaches of

small mountainous streams in New Zealand. The best application of these equations would

be for reaches similar to the ones described in Day (1975).

Jobson (1997) also formulated empirical equations to predict the evolution of a tracer

cloud as it moves downstream. While Day and Wood (1976) developed a dimensionless

curve to represent their dataset, Jobson (1997) modeled the tracer response curve as a scalene

triangle. The peak concentration and the times of arrival of the peak, leading edge, and

trailing are computed with empirical relationships established from time-of-travel studies for

nearly one hundred different rivers and streams. The appeal of using Jobson's method is that

it requires minimal input and the input that is required is typically available through the

United States Geological Society (USGS). Additionally, it is based upon an extensive sample

size so it is not limited to particular types of rivers or channels.

The Dead-Zone Model

The 1-D ADE predicts that the tracer response curve will eventually become

Gaussian at large distances downstream. This behavior is not observed in the results from

tracer studies in natural channels (Nordin and Sabol, 1974; Day, 1975). Tracer profiles from

field tests maintain a degree of asymmetry, even for large distances downstream. Models

that use dead zones as a mechanism to account for the persistent skew seen in tracer response

curves are termed dead zone or transient storage models. The linear growth of the variance

in the main channel is maintained in the dead zone model, but it includes additional terms to

account for persisting skew of the tracer distribution; however, as in Taylor's analysis, the

skew eventually goes to zero. These additional terms describe the movement of tracer in and

out of the dead zone. Assuming that the tracer is well mixed across the channel and within

the dead zones, the transport equations and boundary conditions for the dead zone model are

given by (Hays et al., 1966; Davis et al., 2000; Schmid, 2002; De Smedt, 2006):

$$\frac{\partial C_m}{\partial t} = D\frac{\partial^2 C_m}{\partial x^2} - U\frac{\partial C_m}{\partial x} - \alpha_d(C_m - C_d) \tag{33}$$

$$\beta_d\frac{\partial C_d}{\partial t} = \alpha_d(C_m - C_d) \tag{34}$$

where C_m is the concentration in the main channel, C_d is the concentration in the dead zone,

β_d is a parameter used to describe the ratio of the area of the dead zone to the area of the

main channel, and α_d is the mass exchange coefficient between the main channel and storage

zone. For an instantaneous slug release, the initial conditions are

$$C_m(x, t = 0) = \frac{M_0}{A}\delta(x) \tag{35}$$

$$C_d(x, 0) = 0 \tag{36}$$

where $\delta(x)$ is the Dirac delta function, and the boundary conditions are that the

concentration is zero far from the release point (i.e., $C_m(\infty, t) = 0$), and that for a

conservative tracer the mass passing a point must be equal to the initial mass:

$$UA \int_0^\infty C_m(x, t)dt = M_0. \tag{37}$$

Valentine and Wood (1977) solved for the spatial moments of the dead zone model and studied their behavior with respect to time. From this spatial moment analysis, they came to two major conclusions regarding the effect of dead zones in channels: (1) dead zones increase the magnitude of the longitudinal dispersion; and (2) dead zones increase the advective length.

Bencala and Walters (1983) numerically solved Eq. 33 and 34 and fit their solution to field tracer measurements. Others have expanded upon this numerical solution, including Runkel and Chapra (1993); their numerical solution was used to create the One-dimensional Transport with Inflow and Storage (OTIS; http://co.water.usgs.gov/otis) model.

The analytical solution to the dead zone system of equations was obtained using Laplace transforms by Davis et al. (2000) and De Smedt et al. (2005). Because it is simpler and requires fewer steps, De Smedt's (2005) derivation is provided. The Laplace transform $\tilde{f}(s)$ of a function $f(t)$ is defined as

$$\bar{f}(s) = L\{f(t)\} = \int_0^\infty f(t)e^{-st}dt \tag{38}$$

where s is the transform variable. The Laplace transform is applied to Eq. 33 and 34 so that

$$D\frac{\partial^2 \bar{C}_m}{\partial x^2} - U\frac{\partial \bar{C}_m}{\partial x} - \left(s + \alpha_d - \frac{\alpha^2}{\alpha_d + \beta_d s}\right)\bar{C}_m = \left(\frac{M}{A}\right)\delta(x) \tag{39}$$

$$\bar{C}_s = \frac{\alpha_d \bar{C}_m}{\alpha_d + \beta_d s} \tag{40}$$

When α_d or β_d are zero, Eq. 43 and 44 reduce to the transformed expression of the 1-D ADE. Recall that the analytical solution to 1-D ADE was given by Eq.18. The transformed concentration can be written in terms of Eq.18:

$$\bar{C}_m(x,s) = \bar{C}_0\left(x, s + \alpha_d - \frac{{\alpha_d}^2}{\alpha_d + \beta_d s}\right) \tag{41}$$

The convolution theorem of the Laplace transform presented by Sneddon (1972, p. 228) was used to find the solution to Eq. 45. In order to apply this theorem, Eq. 41 is re-written as a function of three variables: x, s_1 and s_2:

$$\bar{C}_m(x, s_1, s_2) = \bar{C}_0\left(x, s_1 + \alpha_d - \frac{\alpha_d{}^2}{\alpha_d + \beta_d s_2}\right) \qquad (42)$$

The inverse Laplace transform of Eq. 46 is determined with respect to s_1 and then again with respect to s_2. After it is inverted with respect to s_1, Eq. 42 becomes

$$L\{C_m(x, t_1, t_2)\} = C_0(x, t_1) e^{-\alpha_d t_1} e^{\frac{\alpha_d^2 t_1}{\alpha_d + \beta_d s_2}} \qquad (43)$$

Taking the inverse Laplace transform with respect to s_2 gives

$$C_m(x, t_1, t_2) = C_0(x, t_1) e^{-\alpha_d t_1} e^{-\frac{\alpha_d}{\beta_d} t_2} L^{-1}\left[e^{\frac{\alpha_d^2 t_1}{\beta_d s_2}} \right] \qquad (44)$$

Next, the convolution theorem is applied. The final solution is written as

$$C_m(x, t) = \int C_1(x, \tau) e^{-\alpha_d \tau - \frac{\alpha_d}{\beta_d}(t - \tau)} \left[\frac{\alpha_d}{\beta_d} \sqrt{\frac{\beta_d}{t_2}} I_1\left(2\alpha_d \sqrt{\frac{\tau(t - \tau)}{\beta_d}} \right) + \delta(t - \tau) \right] d\tau \qquad (45)$$

De Smedt et al. (2005) compared their analytical solution with the OTIS-model solution and found it to agree; any discrepancies between the analytical solution and the numerical solution were due to numerical error generated in OTIS (De Smedt et al., 2005). The analytical solution from Davis et al. (2000) was compared to experimental data in a laboratory flume. Measurements were taken at various lengths, two within the advective zone. The predicted peak concentrations for the two locations in the dead zone exceeded the measured values by two orders of magnitude; the model predicted within an order of magnitude for locations after the advective length (Refer to Fig. 8 in Davis et al., 2000).

These results indicate that the analytical solution to the dead zone model is appropriate for distances outside of the advective zone but it is not appropriate within the advective zone.

Advective Zone Models

The 1-D ADE does not apply in the advective zone because the tracer has not had sufficient time to reach equilibrium between longitudinal advection and transverse dispersion. An alternative model is necessary, especially for wide rivers where the length of the advective zone is large because of the time required for the tracer to fully mix across the width. A solution to mixing in the advective zone can be described by the unsteady two-dimensional depth-averaged transport equation given by

$$\frac{\partial C}{\partial t} + U\frac{\partial C}{\partial x} + V\frac{\partial C}{\partial y} = D_x\frac{\partial^2 C}{\partial x^2} + D_y\frac{\partial^2 C}{\partial y^2} \qquad (46)$$

where U and V are the depth-averaged longitudinal and transverse velocity components and D_x and D_y are the mixing coefficients in the x and y directions. Mixing with respect to depth is not considered because mixing over the depth occurs much faster than mixing over the width for wide rivers for channels with greater widths than depths. Two-dimensional mixing models for straight channels have numerically solved Eq. 46 for steady (Akhtar, 1978; McCorquodale et al., 1983) and unsteady pollutant input (Verboom, 1974; Holly, 1975; Ohishi, 1981). These models are limited in their use because they describe mixing processes in straight, uniform channels.

For non-uniform, meandering channels Eq. 46 can be replaced with a streamtube model. Instead of using the traditional Cartesian coordinates, the streamtube model uses α_c and β_c, the longitudinal and transverse curvilinear coordinates. The advection/dispersion equation in curvilinear coordinates derived by Chang (1971) is

$$\frac{\partial C}{\partial t} + \frac{v_\alpha}{m_\alpha}\frac{\partial C}{\partial \alpha_c} + \frac{v_\beta}{m_\beta}\frac{\partial C}{\partial \beta_c} = \frac{1}{hm_\alpha m_\beta}\left[\frac{\partial}{\partial \alpha}\left(\frac{m_\beta}{m_\alpha}hk_\alpha\frac{\partial C}{\partial \alpha_c}\right) + \frac{\partial}{\partial \beta_c}\left(\frac{m_\alpha}{m_\beta}hk_\beta\frac{\partial C}{\partial \beta_c}\right)\right] \qquad (47)$$

where v_α and v_β are depth-averaged longitudinal and transverse velocities, k_α and k_β are the

longitudinal and transverse dispersion coefficients, and m_α and m_β are metric coefficients

that describe the non-uniformity of the channel in the longitudinal and transverse direction. It

is assumed that v_β is zero. When m_α and m_β are equal to 1, the channel straight and has zero

roughness. The streamtube model transforms Eq. 47 with the variable q, the cumulative

discharge:

$$q(\alpha_c, \beta_c) = \int_{-\infty}^{\beta_c} m_\beta \, hv_\alpha d\beta_c' \qquad (48)$$

Writing Eq. 51 in terms of q and integrating with respect to β gives

$$\frac{\partial C}{\partial t} + \frac{v_\alpha}{m_\alpha}\frac{\partial c}{\partial \alpha_c} = \frac{1}{hm_\alpha m_\beta}\frac{\partial}{\partial \alpha_c}\left(\frac{m_\beta}{m_\alpha}hk_\alpha\frac{\partial c}{\partial \alpha_c}\right) + \frac{v_\alpha}{m_\alpha}\frac{\partial}{\partial q}\left(m_\alpha h^2 v_\alpha k_\beta\frac{\partial C}{\partial q}\right) \qquad (49)$$

As we assumed in Taylor's analysis, the longitudinal diffusion term is very small and can be

eliminated. This reduces Eq. 49 to

$$\frac{\partial C}{\partial t} + \frac{v_\alpha}{m_\alpha}\frac{\partial C}{\partial \alpha_c} = \frac{v_\alpha}{m_\alpha}\frac{\partial}{\partial q}\left(m_\alpha h^2 v_\alpha k_\beta\frac{\partial C}{\partial q}\right) \qquad (50)$$

This equation assumes that tracer input is not steady. If the pollutant input is constant, the

first term is eliminated. Two-dimensional streamtube models have been numerically solved

for the case of steady-state pollutant input (Yotsukura and Sayre, 1976; Lau and

Krishnappan, 1981; Somlyoda, 1982 and Gowda, 1984) and unsteady input (Holly, 1975;

Harden and Shen, 1979; and Luk et al., 1990).

Luk et al. (1990) verified their numerical model with laboratory measurements within

the advective zone. For a slug injection, their predicted results for the peak concentration

were within 5% of the measured results. Although the predicted peak results are in fairly

good agreement with the measured results, Luk et al. did not quantify errors associated with other aspects of the concentration curve, such as the arrival time, variance, and skew. Additionally, the numerical model requires several input parameters including depth measurements across numerous cross sections, velocity and/or discharge measurements, and a measurement of the transverse dispersion coefficient. Obtaining representative values for these parameters is difficult and costly.

A two-parameter one-dimensional model for mixing in the advective zone was developed and evaluated by Reichert and Wanner (1991). This model is termed the 'enhanced one-dimensional model' and is based on a simplified velocity profile consisting of a flowing zone and a stagnant zone with zero velocity (Fig. 2.1). Because the stagnant zone occupies a fraction α of the width, the velocity in the flowing zone is $\overline{U}/(1-\alpha)$. In other dispersion models, such as Taylor's and Jobson's, the velocity is set as the average velocity, $\overline{U}$, for every lateral distance across the stream profile. An illustration of the two assumptions is given in Fig. 2.1; Reichert and Wanner's assumption is a much better fit to the measured data. The model of Reichert and Wanner (1991) includes advection in the flowing zone and transfer between the two zones at a rate q_e. The transport equations of the enhanced one-dimensional model for the concentration C_1 in the flowing zone and C_2 in the stagnant zone are

$$\frac{\partial}{\partial t}[(1-\alpha)AC_1] + \frac{\partial}{\partial x}(QC_1) = -q_e(C_1 - C_2) \tag{51}$$

$$\frac{\partial}{\partial t}(\alpha AC_2) = q_e(C_1 - C_2) \tag{52}$$
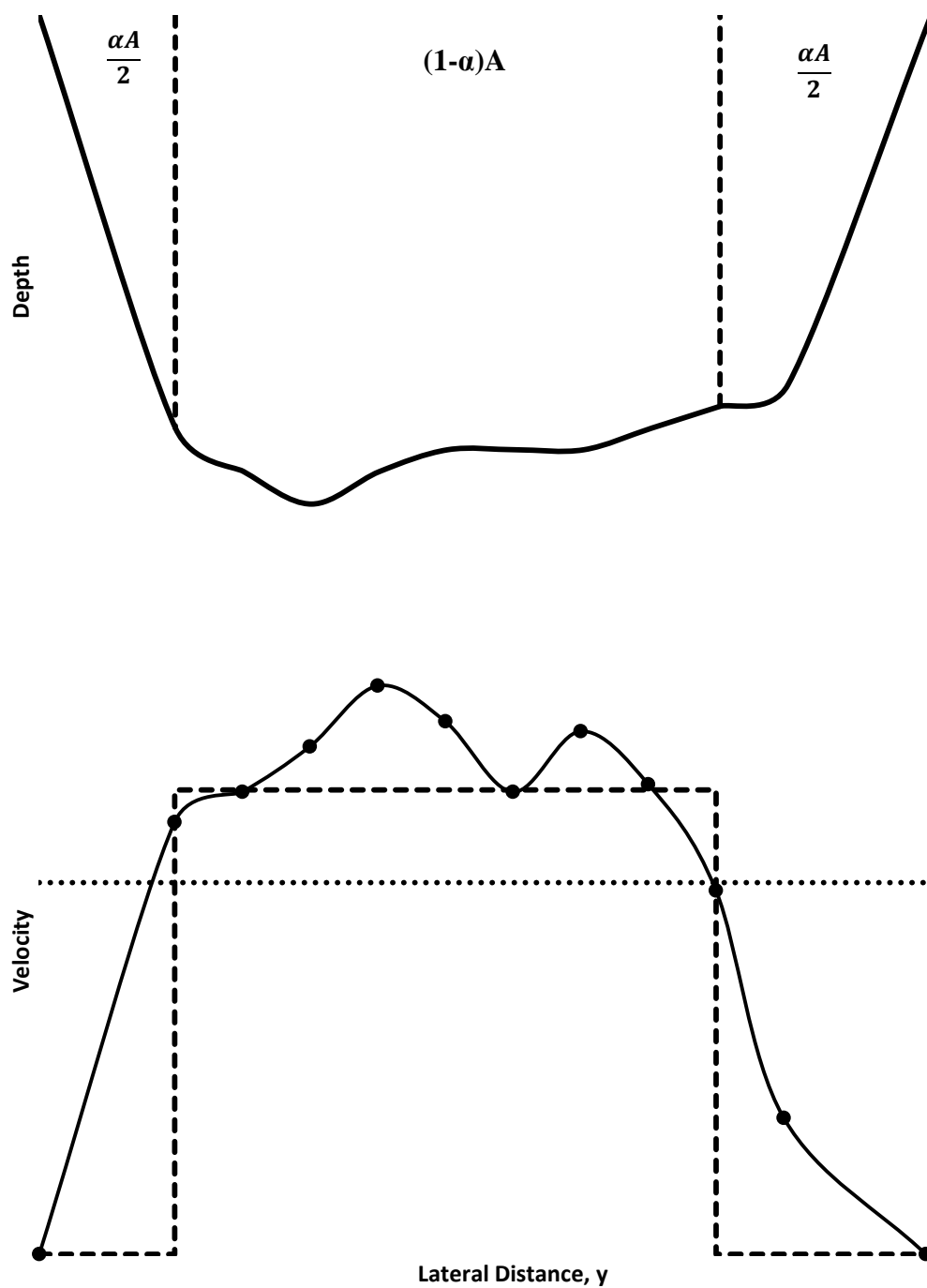
Figure 2.1: Description of channel cross section and velocity profile of Reichert and Wanner model: (a) Portion of the channel defined by as the flowing zone and the stagnant zone. (b) Velocity, U, with respect to transverse location y for measured data (-●-), average velocity, $\bar{U}$, (dotted line), and $\bar{U}/(1-\alpha)$. Measurements were taken at Walnut Creek, Ames, IA.

The transport equations given by this model are similar to the transport equations given by Eq. 33 and 34; the main difference is that the dispersion term is eliminated. Once the concentrations in each zone are computed, the cross-sectional average concentration C is

$$C = (1-\alpha)C_1 + \alpha C_2 \tag{53}$$

Reichert and Wanner (1991) provided guidance for estimating the parameters α and q_e. They showed that with the velocity profile in Fig. 2.1 when applied to Eq. 15 gives

$$K = \frac{\alpha^2}{12} \frac{B^2 \bar{U}^2}{\varepsilon_y}, \tag{54}$$

and they also used the asymptotic behavior of the model to show that

$$K = \frac{\alpha^2 \bar{U}^2}{q_e A}. \tag{55}$$

Equating Eq. 54 and 55 yields

$$q_e = 12\varepsilon_y \frac{h}{B} \tag{56}$$

and with Eq. 27, q_e can be written in terms of the shear velocity, $u*$ so that:

$$q_e = 12\theta \frac{u* h^2}{B} \tag{57}$$

For estimating α, Reichert and Wanner (1991) noted that an analysis of field data gave a range of $0.07 < \alpha < 0.17$ (Nordin and Sabol, 1974); they also used Eq. 54 and Fischer's (1975) formula for the dispersion coefficient (Eq.30) to obtain an approximate formula for α.

$$c_f = \frac{\alpha^2}{12\theta} \tag{58}$$

In the advective zone, transverse mixing is an important process for controlling the transport of material because the concentration is not yet well mixed across the channel.

Reichert and Wanner (1991) model transverse mixing through the exchange between two zones; however, transverse mixing is not accounted for within the individual zones. This simplification can be problematic if the initial input is in the form of a spike or narrow pulse because the model underestimates the lateral exchange in the center of the channel immediately downstream of the initial input (Reichert and Wanner, 1991). In this case, the initial pulse is retained in the flowing zone instead of being dispersed across the channel. Reichert and Wanner (1991) used cosine-squared to describe the shape of the initial pulse. The width of the initial pulse, Δx, is described Reichert and Wanner as the width at half-maximum and with the equation:

$$\Delta x = \gamma_p \alpha \frac{\overline{U} B^2}{\varepsilon_y} \tag{59}$$

where γ_p is a dimensionless coefficient. For the condition $\gamma_p \approx 1/8$, the spike will not appear in the results because it is sufficiently large for the pulse to disperse across the channel and not stay in the flowing zone. Reichert and Wanner verified this conclusion by plotting the solution of their model with respect to dimensionless distance defined by:

$$x' = \frac{\varepsilon_y}{\overline{U} B^2} x \tag{60}$$

When $\gamma_p \leq 1/8$, a spike will be present in the results for C vs. x', however it will be significantly smaller at $x'=0.2$ and disappears completely by $x' = 0.4$ (Reichert and Wanner, 1991). In addition to understanding the behavior of the initial pulse, Reichert and Wanner compared their solution to measured data recorded by Nordin and Sabol (1974). They found that the solution was in good agreement with the measured results after $x' = 0.8$; before this distance the model under predicted the peak concentration and over predicted the variance.

Although Reichert and Wanner (1991) presented the concentration curves produced with their model in their results, they did not show how the solution was derived. Their solution has the potential of being extremely useful to water resource engineers and scientists because the advective length can be quite large in natural channels. Additionally, Reichert and Wanner showed that their model was able to predict the concentration for most of the advective length without adding several additional terms to account for lateral mixing. In fact, the Reichert and Wanner model only requires one additional term than Taylor's dispersion model.

Summary

For most cases, describing longitudinal dispersion with Taylor's analysis is a good first approximation. Several researchers have taken Taylor's analysis and expanded upon the 1-D advection-dispersion equation (Eq. 17) by deriving a solution to the equation, modifying the original equation to include additional parameters to account for channel features and/or irregularities, or creating empirical equations to estimate the coefficients of the equation. These developments have greatly improved the ability for researchers to model longitudinal dispersion for a variety of channels; furthermore, users have the ability to choose the solution that best fits their needs based on the resources available and the precision needed.

There are some cases where it is not possible to use Taylor's analysis or using Taylor's analysis results in greater error than desired. In these cases, alternative models are pursued. Taylor's analysis cannot be used in cases where there are insufficient resources to reasonably predict dispersion coefficients, such as remote locations; instead, empirical models are used because they require very little input to estimate contaminant transport.

Empirical models are helpful when resources are sparse, but they simplify the physical processes describing dispersion and these simplifications may lead to large errors. Alternative theoretical transport equations have been developed for the several models including the dead zone model, the streamtube model and Reichert and Wanner's. The transport equations for these models are closely related to Taylor's transport equations; however, additional terms are added to account for processes not included in Taylor's model. These additional terms can be used to describe the transport in and out of dead zones or describe on-going lateral exchange within the advective zone. When applied to field data, these models often predict contaminant transport better than Taylor's model; however, they are criticized because it is difficult to define their additional terms. This is especially true for 2D advective zone models. A water quality modeler has the option of using Taylor's model that may result in large errors, or they can use the streamtube model that requires six parameters per streamtube to be identified in general. Reichert and Wanner's model is an attractive alternative to the streamtube model because it only requires one additional parameter to identify and the parameters can be related to Taylor's dispersion parameter, K; however, the user must solve the set of PDEs given by the transport equations.

An enhanced understanding of the processes controlling longitudinal dispersion in addition to the development of solutions to explain these processes with the resources allotted will result in improved estimation of contaminant transport.

CHAPTER 3: METHODS

Introduction

The one-dimensional dispersion model presented by Reichert and Wanner (1991) has far fewer parameters to define than two-dimensional models applicable within the advective zone, and compared to other one-dimensional models, it has just one more coefficient than the Taylor model and one fewer than the dead zone model. The Reichert and Wanner model is simple, and it can be extremely useful to water quality engineers and scientists if a published solution to the transport equations were available. Reichert and Wanner (1991) present concentration curves predicted with their model, but do not explain how the curves were generated. This chapter outlines how an analytical solution to the Reichert and Wanner model was developed, verified, and applied.

Model Development

Contaminant transport in the advective zone depends on velocity differences and transverse mixing. In the streamtube model, the channel is divided into sections based upon the mean velocity. The Reichert and Wanner model (1991) is similar, but it uses only two sections: a flowing zone and a stagnant zone. Although Reichert and Wanner's model does not apply to the entire advective zone (refer to Chapter 2), it requires much less user input than the streamtube model. The transport equations for this model form the basis for the development of the analytical advective zone model.

The cross-sectional area in the advective zone is assumed to remain approximately constant, so Eq. 51 and 52 can be re-written as

$$(1-\alpha)\frac{\partial C_1}{\partial t} + \overline{U}\frac{\partial C_1}{\partial x} = -\beta(C_1 - C_2) \qquad (61)$$

$$\alpha\frac{\partial C_2}{\partial t} = \beta(C_1 - C_2) \qquad (62)$$

where β is defined as

$$\beta = \frac{q_e}{A} \qquad (63)$$

The initial conditions assume an instantaneous Gaussian pulse injection with spread of width

σ_0 into the flowing zone at time $t = 0$ and at location $x = 0$. This condition can be described

by

$$C_1(x,0) = C_0 e^{\left(-x^2/\sigma_0^2\right)} \qquad (64)$$

Additionally, the concentration in the stagnant zone is taken to be zero initially:

$$C_2(x,0) = 0 \qquad (65)$$

The solution to Eq. 61 and 62 is obtained using Laplace transforms. The Laplace transform

of the concentration in the jth zone is

$$\overline{C}_j = \int_0^\infty e^{-st} C_j(x,t)dt \qquad (66)$$

Applying Eq. 66 transforms Eq. 61 and 62 into

$$\frac{\partial \overline{C}_1}{\partial x} + \frac{(1-\alpha)s+\beta}{\overline{U}}\overline{C}_1 = \frac{(1-\alpha)}{\overline{U}}C_1(x,0) + \frac{\beta}{\overline{U}}\tilde{C}_2 \qquad (67)$$

$$\overline{C}_2 = \frac{\beta\overline{C}_1 - \alpha C_2(x,0)}{\alpha s + \beta} \qquad (68)$$

because the Laplace transform of the derivative is

$$L\left(\frac{\partial C_1}{\partial t}\right) = \int_0^\infty e^{-st}\frac{\partial C_1}{\partial t}dt = s\overline{C}_1 - C_1(x,0) \tag{69}$$

Using Eq. 68 to eliminate $\tilde{C}_2$ from Eq. 67 gives

$$\overline{U}\frac{\partial \overline{C}_1}{\partial x} + \left[(1-\alpha)s + \beta - \frac{\beta^2}{\alpha s + \beta}\right]\overline{C}_1 = (1-\alpha)C_1(x,0) + \frac{\alpha\beta}{\alpha s + \beta}C_2(x,0) \tag{70}$$

If $\beta = 0$, Eq. 70 has the solution

$$C_1 = C_0 e^{\left(\frac{-1}{\sigma_0^2}\left(x-\frac{\overline{U}t}{1-\alpha}\right)^2\right)} = N(x,t) \tag{71}$$

The Laplace transform of the solution, $N(x, t)$, is written as $\widetilde{N}(x, s)$. When $\beta \neq 0$, the Laplace

transform for the concentration in the flowing zone can be written as

$$\overline{C}_1(x,s) = \overline{N}(x,s') \tag{72}$$

where

$$s' = s + \frac{\beta}{1-\alpha}\left(1 - \frac{\beta}{\alpha s + \beta}\right) \tag{73}$$

Eq. 72 is inverted using an iterative convolution theorem from Sneddon (1972, p. 228):

$$L\left[\int_0^t f(\tau, t-\tau)d\tau; t \to s\right] = L\{L[f(t_1, t_2); t_2 \to s]t_1 \to s\} \tag{74}$$

De Smedt et al. (2005) used Eq. 74 to invert an expression similar to Eq. 72 in their

derivation of an analytical solution of the dead zone model. Following De Smedt et al.

(2005), Eq. 71 is written as a function of three variables: x, s_1, and s_2, so that

$$\overline{C}_1(x, s_1, s_2) = \overline{N}\left(x, \left(s_1 + \frac{\beta}{1-\alpha}\right) - \frac{\beta^2}{(\alpha s_2 + \beta)(1-\alpha)}\right) \tag{75}$$

The inverse Laplace transform of Eq. 75 is derived iteratively, first with respect to s_1:

$$\overline{C}_1(x,t_1,s_2) = N(x,t_1)e^{\left(\frac{-\beta t_1}{1-\alpha}\right)}e^{\left(\frac{\beta^2 t_1}{(\alpha s_2 + \beta)(1-\alpha)}\right)} \tag{76}$$

This solution was obtained after applying the identity

$$L\left(e^{at} f(t)\right) = \overline{f}(s-a) \tag{77}$$

Next, Eq. 76 is inverted with respect to s_2:

$$C_1\left(x,t_1,t_2\right) = N(x,t_1)e^{\left(\frac{-\beta t_1}{1-\alpha}\right)}e^{\left(\frac{-\beta t_2}{\alpha}\right)}L^{-1}\left[e^{\left(\frac{\beta^2 t_1}{\alpha(1-\alpha)s_2}\right)}\right] \tag{78}$$

The final term of Eq. 78 is solved with the transform relation given by

$$L^{-1}\left[e^{\lambda/s}\right] = \sqrt{\lambda/t}\,I_1\left(2\sqrt{\lambda t} + \delta(t)\right) \tag{79}$$

where λ is

$$\lambda = \frac{\beta^2 t_1}{\alpha(1-\alpha)} \tag{80}$$

The expression for C_1 can be written as

$$C_1(x,t_1,t_2) = N\left(x,t_1\right)e^{\left(\frac{-\beta t_1}{1-\alpha}\right)}e^{\left(\frac{-\beta t_2}{\alpha}\right)}$$
$$\times\left[\sqrt{\frac{\beta^2 t_1}{\alpha(1-\alpha)t_2}}\right]I_1\left(2\sqrt{\frac{\beta^2 t_1 t_2}{\alpha(1-\alpha)}} + \delta(t_2)\right) \tag{81}$$

Eq. 81 is in a form appropriate to apply the convolution theorem. The solution for $C_1(x,t)$ is

$$C_1(x,t) = \int_0^\infty N(x,\tau)e^{\left(\frac{-\beta\tau}{1-\alpha}\right)}e^{\left(\frac{-\beta(t-\tau)}{\alpha}\right)}$$
$$\times\left[\sqrt{\frac{\beta^2\tau}{\alpha(1-\alpha)(t-\tau)}}I_1\left[2\sqrt{\frac{\beta^2\tau(t-\tau)}{\alpha(1-\alpha)}}\right] + \delta(t-\tau)\right]d\tau \tag{82}$$

Substituting Eq. 71 into Eq. 82 and using the properties of the Dirac delta function yields

$$C_1(x,t) = C_0 \left[\left[\left[e^{\left(-\frac{1}{\sigma_0^2}\left(x-\frac{\overline{U}t}{1-\alpha}\right)^2\right)} \right] e^{\frac{\beta t}{1-\alpha}} + \int_0^t e^{\left(-\frac{1}{\sigma_0^2}\left(x-\frac{\overline{U}\tau}{1-\alpha}\right)^2\right)} e^{\frac{-\beta\tau}{1-\alpha}} e^{-\frac{\beta(t-\tau)}{\alpha}} \right.\right.$$

$$\left.\left. \times \sqrt{\frac{\beta^2\tau}{\alpha(1-\alpha)(t-\tau)}} I_1\left[2\sqrt{\frac{\beta^2\tau(t-\tau)}{\alpha(1-\alpha)}}\right] d\tau \right] \right] \tag{83}$$

The solution to C_1 contains two main components—the first term contains the initial

Gaussian pulse and the second term contains an indefinite integral. Recall that the average

concentration in the channel, C, defined by Eq. 53, is a function of C_1 and C_2. Therefore, an

expression for C_2 must be derived as well. Given the result in Eq. 72, Eq. 68 can be re-

written as

$$\overline{C}_2 = \frac{\beta}{\alpha s + \beta}\overline{C}_1(x,s) = \frac{\beta}{\alpha s + \beta}\tilde{N}(x,s') \tag{84}$$

This expression can be written as the product of two functions, $g(s)$ and $f(s)$, defined by

$$g(s) = \frac{\beta}{\alpha s + \beta} \tag{85}$$

and

$$f(s) = \overline{N}\left(x, s + \frac{\beta}{1-\alpha}\left(1 - \frac{\beta}{\alpha s + \beta}\right)\right) \tag{86}$$

The inverse Laplace transforms, $g(t)$ and $f(t)$, of $g(s)$ and $f(s)$ are

$$L^{-1}[g(s)] = C_1(x,t) \tag{87}$$

$$L^{-1}[f(s)] = \frac{\beta}{\alpha}e^{\frac{-\beta t}{\alpha}} \tag{88}$$

The inverse transform of a product is solved with the convolution theorem:

$$L^{-1}\left[f(s)g(s)\right]=\int_0^t f(\tau)g(t-\tau)d\tau \tag{89}$$

After Eq. 89 is applied, $C_2(x, t)$ can be written as

$$C_2(x,t)=C_0\frac{\beta}{\alpha}\left[\left[\int_0^t e^{\frac{-\beta\tau_2}{\alpha}}e^{\frac{-1}{\sigma^2}\left(x-\frac{\overline{U}(t-\tau_2)}{1-\alpha}\right)^2}e^{\frac{-\beta(t-\tau_2)}{1-\alpha}}\right]d\tau_2+\right.$$

$$\int_0^t\left[e^{\frac{-\beta\tau_2}{\alpha}}\int_0^{t-\tau_2}\left[e^{\frac{-\beta(t-\tau_2-\tau_1)}{\alpha}}e^{\frac{-1}{\sigma_0^2}\left(x-\frac{\overline{U}\tau_1}{1-\alpha}\right)^2}e^{\frac{-\beta\tau_1}{1-\alpha}}\right.\right.$$

$$\left.\left.\left.\times\sqrt{\frac{\beta^2\tau_1}{\alpha(1-\alpha)(t-\tau_2-\tau_1)}}I_1\left[2\sqrt{\frac{\beta^2\tau_1(t-\tau_2-\tau_1)}{\alpha(1-\alpha)}}\right]\right]d\tau_1\right]d\tau_2\right] \tag{90}$$

The solution to C_2, like C_1, contains two main components: the first term contains a single integral and the second term with a double indefinite integral. This solution can be simplified given the definition for the time of advection, t_a

$$t_a=\frac{x(1-\alpha)}{\overline{U}} \tag{91}$$

When Eq. 91 is substituted into Eq. 90; it becomes

$$C_2(x,t)=C_0\frac{\beta}{\alpha}\left[\left[\int_0^t e^{\frac{-\beta\tau_2}{\alpha}}e^{\frac{-1}{\sigma^2}\left(\frac{t_a-\overline{U}(t-\tau_2)}{1-\alpha}\right)^2}e^{\frac{-\beta(t-\tau_2)}{1-\alpha}}\right]d\tau_2+\right.$$

$$\int_0^t\left[e^{\frac{-\beta\tau_2}{\alpha}}\int_0^{t-\tau_2}\left[e^{\frac{-\beta(t-\tau_2-\tau_1)}{\alpha}}e^{\frac{-1}{\sigma_0^2}\left(\frac{t_a-\overline{U}\tau_1}{1-\alpha}\right)^2}e^{\frac{-\beta\tau_1}{1-\alpha}}\right.\right.$$

$$\left.\left.\left.\times\sqrt{\frac{\beta^2\tau_1}{\alpha(1-\alpha)(t-\tau_2-\tau_1)}}I_1\left[2\sqrt{\frac{\beta^2\tau_1(t-\tau_2-\tau_1)}{\alpha(1-\alpha)}}\right]\right]d\tau_1\right]d\tau_2\right] \tag{92}$$

Given the solution from Eq. 82 and Eq. 92 the total concentration in the channel, C, is

$$C(x,t) = C_0 \left[(1-\alpha) \left[e^{-\frac{1}{\sigma_0^2}\left(x-\frac{\bar{U}t}{1-\alpha}\right)^2} e^{-\frac{\beta t}{1-\alpha}} + \int_0^t \left[e^{-\frac{1}{\sigma_0^2}\left(x-\frac{\bar{U}t}{1-\alpha}\right)^2} e^{\frac{-\beta\tau}{1-\alpha}} e^{-\frac{\beta(t-\tau)}{\alpha}} \right. \right. \right.$$

$$\times \sqrt{\frac{\beta^2\tau}{\alpha(1-\alpha)(t-\tau)}} I_1 \left[2\sqrt{\frac{\beta^2\tau(t-\tau)}{\alpha(1-\alpha)}} \right] d\tau \Bigg] \Bigg] +$$

$$\frac{\beta}{\alpha} \left[\int_0^t \left[e^{\frac{-\beta\tau_2}{\alpha}} \int_0^{t-\tau_2} \left[e^{\frac{-\beta(t-\tau_2-\tau_1)}{\alpha}} e^{\frac{-1}{\sigma_0^2}\left(\frac{t_a-\bar{U}\tau_1}{1-\alpha}\right)^2} e^{\frac{-\beta\tau_1}{1-\alpha}} \right. \right. \right.$$

$$\times \sqrt{\frac{\beta^2\tau_1}{\alpha(1-\alpha)(t-\tau_2-\tau_1)}} I_1 \left[2\sqrt{\frac{\beta^2\tau_1(t-\tau_2-\tau_1)}{\alpha(1-\alpha)}} \right] d\tau_1 \Bigg] d\tau_2 \Bigg] \Bigg]$$

(93)

The solution for C contains four main components—two from C_1 and two from C_2. Three terms contain a convolution integral which require numerical integration to solve. With numerical integration, the smaller the integrating unit is, the more precise the solution will be; however, it will take longer to compute the solution. Values of C, C_1 and C_2 were computed using MATLAB (R2012a, Mathworks, 2012). To compute a time series of concentration, the functions in Appendix A requires the user to specify the number of time steps. Similarly, to compute the integrals over τ, the user must specify the number of points at which the integrand is computed. The solution given by C is checked by methods described in the next section.

Model Verification

To verify the analytical solution, the moments of Eq. 93 are compared to the spatial and temporal moments of the Reichert and Wanner model.

Spatial Moment Analysis

The zeroth, first, second, and third spatial moments of the concentration distribution predicted by the Reichert and Wanner model were derived for the flowing zone and the stagnant zone in order to obtain analytical expressions for the mass M, spatial center of mass μ_x, spatial variance σ_x^2, and spatial skew γ_x. The analytical solutions for M, μ_x, σ_x^2, and γ_x were compared to the values acquired by integrating the spatial concentration curves calculated by Eq. 93. The general expression for the nth spatial moment for each zone is given as (a modification of Eq. 19):

$$F_{nx} = \int_{-\infty}^{\infty} x^n C_1 dx \tag{94}$$

$$S_{nx} = \int_{-\infty}^{\infty} x^n C_2 dx \tag{95}$$

where F_{nx} is the nth spatial moment in the flowing zone and S_{nx} is the nth spatial moment in the stagnant zone. To derive equations for the evolution of the spatial moments, Eq. 61 and 62 are multiplied by x^n and integrated over all x. The advection term in Eq.61 must be integrated by parts:

$$U \int_{-\infty}^{\infty} x^n C_1 dx = U \left(x^n C_1 \Big|_{-\infty}^{\infty} - \int_{-\infty}^{\infty} n x^{n-1} C_1 dx \right) = -n U F_{nx-1} \tag{96}$$

Then, the transport equations for the nth moments are

$$(1-\alpha)\frac{dF_{nx}}{dt} + \beta(F_{nx} - S_{nx}) = nUF_{nx-1} \tag{97}$$

$$\alpha \frac{dS_{nx}}{dt} - \beta(F_{nx} - S_{nx}) = 0 \tag{98}$$

Eq. 97 and 98 are used to set a system of ordinary differential equations (ODEs) for the first

four spatial moments. For an instantaneous injection of Gaussian pulse in the flowing zone

at $x = 0$ (Eq. 64), the initial conditions are

$$F_{0x}(0) = \frac{M_0}{1-\alpha}, \quad F_{2x}(0) = \frac{M_0\sigma_0^2}{1-\alpha},$$
$$S_{0x}(0) = F_{1x}(0) = S_{1x}(0) = S_{2x}(0) = F_{3x}(0) = S_{3x}(0) = 0 \tag{99}$$

where M_0 is the initial mass of the tracer and σ_0^2 is the initial spatial variance of the tracer

pulse. The solution for the first four spatial moments in each zone—F_{0x}, S_{0x}, F_{1x}, S_{1x}, F_{2x}, S_{2x},

F_{3x}, S_{3x}—was obtained by solving the linear system of ODEs defined by Eq. 97 and 98 given

their corresponding initial conditions (Eq. 99). The composite solution for the nth moment is

defined as:

$$M_{nx} = (1-\alpha)F_{nx} + \alpha S_{nx} \tag{100}$$

The composite moments were used to form analytical expressions for M, μ_x, σ_x^2, and γ_x:

$$M(t) = M_0 \tag{101}$$

$$\mu_x(t) = -\frac{U\left(\alpha^2 e^{\frac{\beta t}{\alpha(-1+\alpha)}} - \alpha^2 - \beta t\right)}{\beta} \tag{102}$$

$$\sigma_x^2(t) = -\frac{1}{(-1+\alpha)\beta^2}\left[\left(4\alpha^3\beta e^{\frac{\beta t}{\alpha(-1+\alpha)}}\overline{U}^2\,2\alpha^2\overline{U}^2\beta e^{\frac{\beta t}{\alpha(-1+\alpha)}} + 2\beta\alpha^2\overline{U}^2\right.\right.$$
$$\left.-2\alpha^3\overline{U}^2\beta\right)t\right] - \left[\overline{U}^2\alpha^5 e^{\frac{2\beta t}{\alpha(-1+\alpha)}} + \overline{U}^2\alpha^4 e^{\frac{2\beta t}{\alpha(-1+\alpha)}} + 4\alpha^3\overline{U}^2 e^{\frac{\beta t}{\alpha(-1+\alpha)}}\right.$$
$$-8\alpha^4\overline{U}^2 e^{\frac{\beta t}{\alpha(-1+\alpha)}} + 4\alpha^5\overline{U}^2 e^{\frac{\beta t}{\alpha(-1+\alpha)}} + 9\alpha^4\overline{U}^2 - 4\alpha^3\overline{U}^2 - 5\alpha^5\overline{U}^2$$
$$\left.-\alpha\beta\sigma_0^2 + \beta^2\sigma_0^2\right] / \left[(-1+\alpha)\beta^2\right] \tag{103}$$

$$\gamma_x(t) = \left[-\frac{1}{\beta^3\left(\alpha^2+1-2\alpha\right)} \left(42\alpha^5\beta\overline{U}^2 e^{\frac{\beta t}{\alpha(-1+\alpha)}}t + 3\alpha^4\beta^2\overline{U}^2 e^{\frac{\beta t}{\alpha(-1+\alpha)}}t^2 \right.\right.$$

$$-18\alpha^4\beta\overline{U}^2 e^{\frac{\beta t}{\alpha(-1+\alpha)}}t - 24\alpha^6\beta\overline{U}^2 e^{\frac{\beta t}{\alpha(-1+\alpha)}}t - 192\alpha^7\overline{U}^2 e^{\frac{\beta t}{\alpha(-1+\alpha)}} + 222\alpha^6\overline{U}^2 e^{\frac{\beta t}{\alpha(-1+\alpha)}}$$

$$-108\alpha^5\overline{U}^2 e^{\frac{\beta t}{\alpha(-1+\alpha)}} + 60\alpha^8\overline{U}^2 e^{\frac{\beta t}{\alpha(-1+\alpha)}} + 18\alpha^4\overline{U}^2 e^{\frac{\beta t}{\alpha(-1+\alpha)}} - 6\alpha^3\beta^2\sigma_0^2 e^{\frac{\beta t}{\alpha(-1+\alpha)}}$$

$$-60\alpha^8\overline{U}^2 - 3\alpha^4\beta^2\sigma_0^2 + 192\alpha^7\overline{U}^2 - 3t\beta^3\sigma_0^2 + 108\alpha^5\overline{U}^2 - 18\alpha^4\overline{U}^2$$

$$-3\alpha^2\beta^2\sigma_0^2 + 6\alpha^3\beta^2\sigma_0^2 - 9t^2\alpha^4\beta^2\overline{U}^2 - 18t^2\alpha^3\beta^2\overline{U}^2 - 9t^2\alpha^4\beta^2\overline{U}^2$$

$$-t^3\beta^3\overline{U}^2 - 222\alpha^6\overline{U}^2 + 3\alpha^4\beta^2\sigma_0^2 e^{\frac{\beta t}{\alpha(-1+\alpha)}} + 3\alpha^2\beta^2\sigma_0^2 e^{\frac{\beta t}{\alpha(-1+\alpha)}} - t^3\alpha^2\beta^3\overline{U}^2$$

$$+2t^3\alpha\beta^3\overline{U}^2 + 90t\alpha^5\beta\overline{U}^2 - 36t\alpha^6\beta\overline{U}^2 + 72t\alpha^4\beta\overline{U}^2 - 18t\alpha^3\beta\overline{U}^2$$

$$\left.-3t\alpha^2\beta^3\sigma_0^2 + 6t\alpha\beta^3\sigma_0^2\right)\overline{U}\right] - \left[3\overline{U}\left(\alpha^2 e^{\frac{\beta t}{\alpha(-1+\alpha)}} - \alpha^2 - t\beta\right)\right.$$

$$\left(\overline{U}^2\alpha^5 e^{\frac{\beta t}{\alpha(-1+\alpha)}} - \overline{U}^2\alpha^4 e^{\frac{\beta t}{\alpha(-1+\alpha)}} + 4\overline{U}^2\alpha^3 e^{\frac{\beta t}{\alpha(-1+\alpha)}} - 8\overline{U}^2\alpha^4 e^{\frac{\beta t}{\alpha(-1+\alpha)}}\right.$$

$$-4\overline{U}^2\alpha^5 e^{\frac{\beta t}{\alpha(-1+\alpha)}} - 4\overline{U}^2\alpha^3\beta e^{\frac{\beta t}{\alpha(-1+\alpha)}}t + 2\overline{U}^2\alpha^2\beta e^{\frac{\beta t}{\alpha(-1+\alpha)}}t - 5\overline{U}^2\alpha^5$$

$$\left.\left.-\alpha\beta^2\sigma_0^2 + 9\overline{U}^2\alpha^4 - 4\overline{U}^2\alpha^3 + 2t\beta\overline{U}^2\alpha^2 + \beta^2\sigma_0^2 - 2t\beta\overline{U}^2\alpha^3\right)\right] /$$

$$\left[-\frac{1}{(-1+\alpha)\beta^2}\left(\alpha^5\overline{U}^2 e^{\frac{2\beta t}{\alpha(-1+\alpha)}} - \alpha^4\overline{U}^2 e^{\frac{2\beta t}{\alpha(-1+\alpha)}}\right.\right.$$

$$\left.\left.\left.+4\alpha^3\overline{U}^2 e^{\frac{\beta t}{\alpha(-1+\alpha)}} - 8\alpha^4\overline{U}^2 e^{\frac{\beta t}{\alpha(-1+\alpha)}}\right)\right]\right]$$

$$(104)$$

The solutions to Eq. 101-104 were generated in MATLAB with *Function 3* (Appendix A).

To verify that the expressions generated by Maple are correct, the solutions from Eq. 101-

104 were checked with a numerical solution. Using the set of ODEs and initial conditions

defined in the spatial moment analysis, the numerical solution was computed using the

MATLAB function *ode45*. This function evaluates non-stiff ODEs through the use of the

fourth-order Runge-Kutta method with a variable time step (R2011b Documentation,

mathworks.com). The functions used for the numerical analysis are *Function 4* and *Function 5* (Appendix A).

Temporal Moment Analysis

The temporal moments of the Reichert and Wanner model function as a secondary verification to the analytical solution given by Eq. 93. The analytical solutions for the temporal moments also are used to determine model parameters, as discussed in Chapter 4. Unlike the spatial moments, the analytical expressions for the temporal moments were not generated by solving a set of ODEs with specified boundary conditions; instead, the analytical expressions were derived using Laplace transforms. Applying the initial and boundary conditions with this approach was simpler than with computing evolution equations for the moments.

Nordin and Troutman (1980) used a relation between the Laplace transform and the moments to compute temporal moments; this relationship was used to derive the expressions for the first four temporal moments in each zone—F_{0t}, S_{0t}, F_{1t}, S_{1t}, F_{2t}, S_{2t}, F_{3t}, S_{3t}; the derivation of these expressions is provided in Appendix B. After the four temporal moments are derived, the method used to derive the composite moments, M_{nt}, as well as expressions for μ_t, σ_t^2, and γ_t is the same as the one used in the spatial moment analysis. The expressions for M_{0t}, μ_t, σ_t^2, and γ_t can be simplified by assuming that x/σ_0 is at least greater than 2. The full expression for M_{0t}, and the simplified expressions for M_{0t}, μ_t, σ_t^2, and γ_t are

$$M_{0t}(x) = (1-\alpha)\frac{C_0\sigma_0\sqrt{\pi}}{U}\left[1-\frac{1}{2}erfc\left(\frac{x}{\sigma_0}\right)\right] \approx (1-\alpha)\frac{C_0\sigma_0\sqrt{\pi}}{U} \tag{105}$$

$$\mu_t(x) = \frac{x}{U} + \frac{\alpha^2}{\beta} \tag{106}$$

$$\sigma_t^2(x) = \frac{2\alpha^2}{U\beta}x + \frac{\alpha^3}{\beta^2}(2-\alpha) \tag{107}$$

$$\gamma_t(x) = \frac{\dfrac{6\alpha^3}{U\beta^2}x + 6(1-\alpha)\dfrac{\alpha^4}{\beta^3} + \dfrac{2\alpha^6}{\beta^3}}{\left[\dfrac{2\alpha^2}{U\beta}x + \dfrac{\alpha^3}{\beta^2}(2-\alpha)\right]^{3/2}} \tag{108}$$

The solutions to Eq. 105-108 were computed with *Function 6* (Appendix A). The numerator

of the skewness coefficient is used in this analysis instead of the skew to simplify

calculations; it is referred to as g_t. Eq. 105-108 are similar to Eq. 101-104 in several ways,

especially for large distances or large times. The mass, *M*, and the zeroth temporal moment,

$M_{0t,}$ are both constants for all time (the units are different, however), and the spatial and

temporal center of mass, μ_x and μ_t, grow linearly as a function of the mean velocity, *U*.

Although it is not as clear, both variances, σ_x^2 and σ_t^2, grow linearly after sufficient time and

distance. Finally, the skewness coefficients, γ_x and γ_t, both approach zero at large distances

and times.

Model Application

The performance of the analytical solution is evaluated by comparing the theoretical

predictions with experimental tracer results measured in the advective zone. Day (1975)

conducted a set of tracer experiments in five braided mountainous stream reaches in New

Zealand. These streams have similar geomorphological characteristics: steep slopes

(>0.015), rough beds (mean sediment size ~10 cm), and low sinuosity (Day, 1975). From

the 49 experiments, 702 time concentration curves were recorded. For this analysis, only the 16 tracer response curves recorded in the Thomas reach on 30 Aug. 1972 are used. These sixteen concentration curves, published in Figure 12 of Day and Wood (1976), were digitized in MATLAB. The first four temporal moments, M_{0t}, M_{1t}, M_{2t} and M_{3t}, of the digitized curve were computed to obtain values for the measured temporal center of mass μ_{tm}, the measured temporal variance $\sigma_{tm}{}^2$, and measured numerator to the temporal skewness coefficient, $g_{tm,}$ for each curve.

The hydraulic characteristics of Thomas Reach are given in Table 3.1. This dataset is useful for evaluating the analytical solution in Eq. 93 because several measurements (if not all, depending on how the L_x is computed) were recorded within the advective length; data sets from other field studies (Jobson, 1997; Nordin and Sabol, 1974; Davis et al., 2000) typically have very few reported measuring locations before the advective length because Taylor's model and the dead zone model do not apply in this region. Additionally, this dataset has been used or referenced in several mixing studies based upon the behavior observed (Bencala and Walters, 1983; Hunt, 1999; Kadlec, 1994).

A 4 L salt solution slug of specified concentration was injected into the thalweg of the Thomas Reach (approximately the center). The concentration was measured at 50, 62.5, 75, 87.5, 100, 125, 175, 200, 225, 250, 275, 300, 350, 400, 450, and 500 m downstream from the initial injection. Concentrations were measured in the center of the channel with a conductivity probe. The initial concentration of the salt slug is not reported in Day (1975); however, Day and Wood (1976) report that integration of the concentration curves accounts for the total mass injected.

Table 3.1: Channel and Hydraulic Data for Thomas Reach on 30.Aug.1972*

Slope (m/m)	0.0273
Mean Sediment Size** (cm)	5.6
Discharge (m^3/s)	0.37
Mean Velocity (m/s)	0.54
Mean Flow Width (m)	3.8
L_x (α*=0.4-1.4)*** (m)	161-563

*Data taken from Table 1 and Table 2 from Day (1975)
**Surface sample by line grid oriented along the channel (Day 1975)
***Range based on values of α^* recommended by Fischer (1966), Chatwin (1972), and Denton (1990)

Two estimates of the advective length, L_x, of Thomas Reach were calculated by Day

(1975) using a form of Eq. 23. The two lengths—161 m and 403 m—were calculated using

recommended values of $\alpha^* = 0.4$ from Fischer (1966) and $\alpha^* = 1$ from Chatwin (1972). At

the time when Day published this paper, Chatwin's estimate of α^* was the most conservative;

however, since then, more research has been done in natural channels and channels with dead

zones. Recall from Chapter 2 these studies predict much greater α^*. When Denton's value of

$\alpha^* = 1.4$ is used, L_x for Thomas Reach is 563 m.

Day (1976) investigated the precision and probable uncertainty associated with the

measurements from the tracer study. The errors for measurements in the Thomas Reach on

30.8.1972 are 13.1% for tracer integral; 4.0% for mean velocity, and 12.4% for discharge.

The error in the tracer integral can be related to the error in concentration measurements.

Estimating Model Parameters

There are several methods ranging from theoretical to empirical used to estimate

mixing parameters. The moment matching method is applied to this model through two

different approaches to estimate $\overline{U}$, α, and β. The first approach assumes $\overline{U}$, α, and β

remain constant throughout the entire reach. Single values of $\overline{U}$, α, and β are extracted from

relationships given by the measured temporal moments and Eq. 105-108. The second

approach optimizes the values for the three coefficients so that the values are specific to each

sub-reach. In the optimized method, the individual temporal moments for the particular

reach are used to approximate values for $\overline{U}$, α, and β.

The analytical solution assumes that the initial injection of tracer is in the form of an

instantaneous Gaussian pulse. Reichert and Wanner's model is sensitive to the relative width

of the initial pulse (see Chapter 2), but it was found that for values of $\sigma_0 > 7.5$ m, the solution

does not contain a large spike. This is the only value that was not estimated from the

measured results.

The 16 values for μ_{tm}, $\sigma_{tm}{}^2$, and g_{tm} were plotted as a function of x; a first-order line

was fit for each parameter set, and the slopes of the lines were used to approximate the

constant coefficient values for $\overline{U}$, α and β. The relationships are given as

$$\overline{U} = b_1 \tag{109}$$

$$\beta = \frac{9}{2} \frac{\overline{U} b_2^3}{b_3^2} \tag{110}$$

$$\alpha = \frac{3}{2} \frac{\overline{U} b_2^2}{b_3} \tag{111}$$

where b_1 is the slope of the best-fit line through μ_{tm}, b_2 is the slope of the best-fit line through $\sigma_{tm}{}^2$ and b_3 is the best-fit line through g_t.

For the optimized method, a line was fit to each value of μ_{tm}, $\sigma_{tm}{}^2$, and g_t through the origin to obtain 16 individual values of b_1, b_2 and b_3. These values are used to compute individual values of $\overline{U}$, α, and β defined as $\overline{U}_i$, α_i, and β_i. Given the optimized values of the mean velocity $\overline{U}_i$, stagnant zone fraction α_i, and the assumed value of σ_0, the initial concentration, C_0 for each location is calculated with

$$C_0 = \frac{M_{0t}\,\overline{U}_i}{\sqrt{\pi}\sigma_0(1-\alpha_i)} \tag{112}$$

The approximation for C_0 is used for both methods. The predicted concentration curves from Taylor's analysis are plotted with respect to the measured data and the predicted data from Eq. 93 so that predictions from both methods can be compared to Day's measured data. Recall that the analytical solution for Taylor's analysis is given by Eq. 18. Values for the four coefficients, M, A, K, and U are equal to or derived from values of $\overline{U}$, α, β and C_0 approximated in the previous analysis, or the parameter values were reported by Day (1975). The mass, M, is predicted by

$$M = \sqrt{\pi}C_0\sigma_0 \tag{113}$$

and the dispersion coefficient, K, is predicted with the expression given by Eq. 55 after substituting in Eq. 63 which gives

$$K = \frac{\alpha^2\overline{U}^2}{\beta} \tag{114}$$

As with the previous analysis, both constant coefficients and optimized values for the values

of M, A, K, and $\overline{U}$ are computed.

CHAPTER 4: RESULTS AND DISCUSSION

Introduction

The predicted concentrations from Eq. 93, as well as Eq. 83 and Eq. 90, are assessed to understand the range of applicability of the solution and the response of the solution to changes in model parameters. The behavior of the temporal and spatial moments predicted by the integration of Eq. 93 is analyzed to verify that it is a solution to the Reichert and Wanner model. Additionally, the behavior of the moments provides insight into the physics of the model. Finally, the solution is applied to field data recorded by Day (1975). The parameters are approximated through a moment matching method where the analytical solutions for the temporal moments are matched with the measured temporal moments. With the parameters $\overline{U}$, α, β, and C_0 predicted from the moment matching method, the predicted concentration curves are plotted with respect to the measured concentration curves. Additionally, the predicted and measured curves are compared with predicted results from Taylor's analysis. For each analytical solution a constant coefficient case and optimized case is analyzed. The results from this analysis are used to assess the value of the analytical solution to the Reichert and Wanner model.

Effect of the Initial Pulse

As described in Chapter 2, Reichert and Wanner (1991) used a cosine-squared initial concentration pulse and specified the width of their pulse to be Δx, which is the width at half-maximum. In the present analysis, the pulse is described as a Gaussian plume with spread σ_0, defined by

$$\sigma_0 = \psi \frac{\alpha U}{\beta} \tag{115}$$

where ψ is a dimensionless coefficient used to describe the relative width of the pulse and is proportional—but not equal to—γ_p.

To understand the behavior of the response curves the results were normalized with respect to concentration, time and space. The dimensionless concentration, C^*, time, t', and space, x' are defined by

$$C^* = \frac{\beta}{12MQ} C \tag{116}$$

$$t' = \frac{\beta}{12} t \tag{117}$$

$$x' = \frac{\beta}{12U} x \tag{118}$$

The purpose of the asterisks in C^* is to distinguish the normalized concentration from the deviation in concentration, C'. At the advective length, L_x, x' is approximately equal to

$$x' = \frac{\alpha^*}{4} \tag{119}$$

given the relationship established in Eq. 23 and assuming an initial injection in the center of the channel. The values in Eq.116-118 correspond to the dimensionless parameters used by Reichert and Wanner (1991).

The dimensionless cross-sectional average concentration, C^*, the concentration in the main channel, C_1^*, and the concentration in the stagnant zone, C_2^*, are plotted with respect to t' and x' (Fig. 4.1). The behavior of the solid ($\psi = 1.5$) lines in Fig. 4.1 describes the movement and exchange of tracer as it moves with respect to time and space. The advective zone is

characterized by skew observed in the form of tails in the spatial and temporal concentration curves (Reichert and Wanner, 1991). Dispersion controls the degree of skew; if the tracer cloud did not disperse, it would advect downstream as a Gaussian pulse. Dispersion separates tracer particles from the centroid; the delayed parcels arrive at later time, or they are located farther upstream. Therefore, the skew is positive for the temporal curves (Figs. 4.1a-c) and negative for the spatial curves (Figs. 4.1d-f). The magnitude of skew decreases as the tracer moves downstream—that is, for larger x' and t'.

For narrower initial pulses the predicted values of $C^{'*}$ and $C_1^{'*}$ show a noticeable spike (dashed lines ($\psi = 0.2$) in Fig. 4.1). An empirical analysis showed that for values of $\psi \geq 1.5$ the model is able to compute the concentration without producing the spike. In the case where $\psi < 1.5$ the spike is likely to be produced by the model; the solution appears unrealistic when the spike is present. Regardless of the initial input, the mass in the spike eventually equilibrates between the two zones for large distances and times downstream; when the spike is no longer observable; the solution to the Reichert and Wanner model appropriately describes the physical processes of the flow. These results are in agreement with Reichert and Wanner (1991) as discussed in Chapter 2. Additionally, for both the temporal and spatial scales, the effect of the spike is greatly reduced by x' and $t' = 0.25$ and completely gone by $t' = 0.41$.
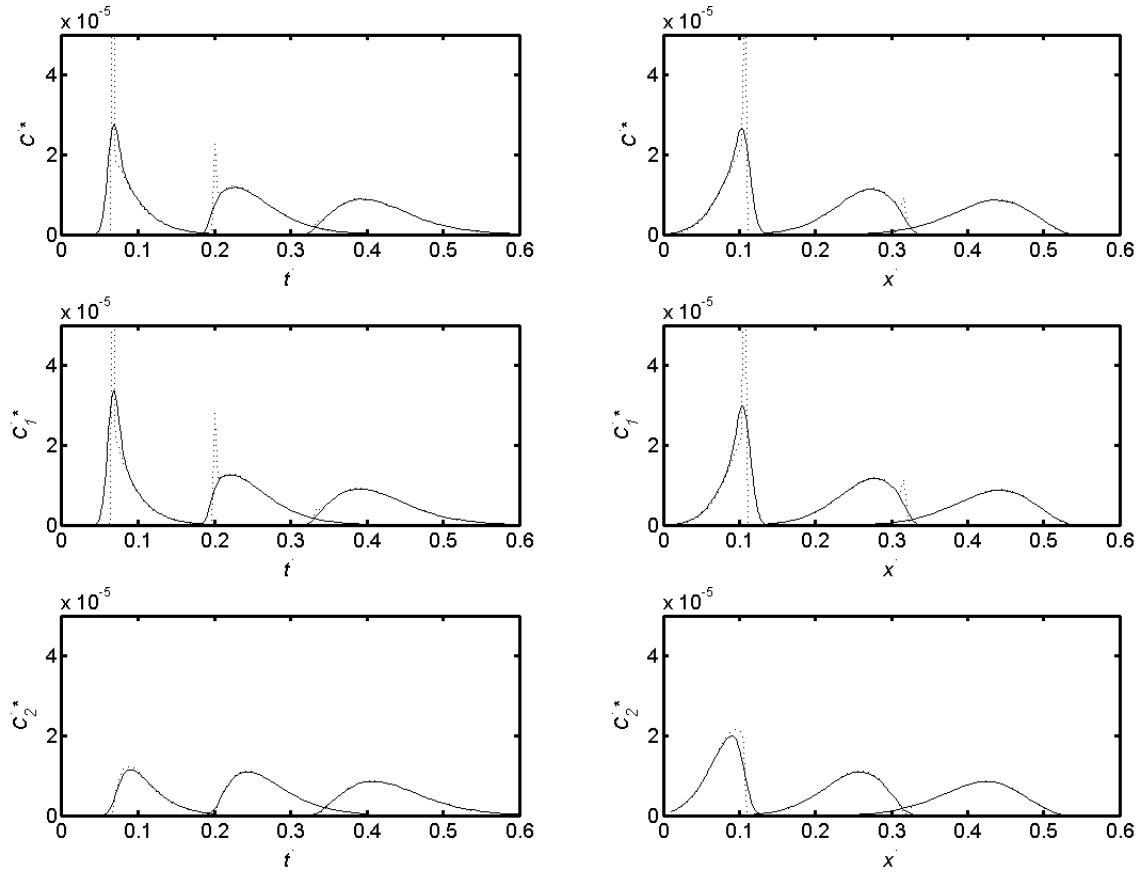
Figure 4.1: Normalized concentration curves. The dashed results represent a narrow initial input with $\psi = 0.2$; solid line results represent a spike of recommended width with $\psi = 1.5$. The left three plots (a-c) are concentration curves as a function of time generated for fixed locations: $x' = 0.08$; $x' = 0.25$; and $x' = 0.41$. The right three plots are concentration curves as a function of space generated for at fixed times: $t' = 0.08$; $t' = 0.25$; and $t' = 0.41$. All six curves were calculated for $\alpha = 0.2$.

Effect of Dispersion Parameters

The parameters α and β control the extent of dispersion in the channel and govern the behavior of the concentration distribution as it moves downstream. Recall that α is the fraction of the channel cross section occupied by the stagnant zone and β describes the exchange rate between the zones. Table 4.1 gives estimated values of α and β based on the

Table 4.1 Representative values of α and β for various rivers based on field measurements

River	h (m)	B (m)	U (m/s)	u* (m/s)	K (m^2/s)	ε_y (m^2/s)	α (--)	β (s^{-1})	U/β (m)
Antietam (USA)	0.39	16	0.32	0.062	9.3	1.45×10^{-2}	0.25	6.8×10^{-4}	4.7×10^2
Manganui (NZ)	0.4	20	0.19	0.18	6.5	4.32×10^{-2}	0.48	1.3×10^{-3}	1.4×10^2
Minnesota (USA)	2.74	80	0.034	0.0024	22.3	3.95×10^{-3}	0.38	7.4×10^{-6}	4.6×10^3
Mississippi (USA)	3.05	530	0.08	0.0056	19.5	1.02×10^{-2}	0.04	4.3×10^{-7}	1.8×10^5
Missouri (USA)	2.33	183	0.89	0.066	465	9.23×10^{-2}	0.14	3.3×10^{-5}	2.6×10^4
Muddy (USA)	0.81	13	0.37	0.081	13.9	3.94×10^{-2}	0.53	2.8×10^{-3}	1.3×10^2
Stony (NZ)	0.63	10	0.55	0.3	13.5	1.13×10^{-1}	0.78	1.3×10^{-2}	4.0×10
Susquehanna (USA)	1.35	203	0.39	0.065	92.9	5.27×10^{-2}	0.10	1.5×10^{-5}	2.5×10^4

relationships given by Eq. 55, 57 and 63and channel geometry and hydraulic measurements presented by Rutherford (1994) in Table. 4.2. For these rivers, α varies 0.04 to 0.78. This range is larger than the range of 0.07-0.17 found by Nordin and Sabol (1974). The estimated values of β vary over almost five orders of magnitude. The exchange coefficient q_e is directly proportional to β, and both parameters are inversely proportional to the transverse mixing time. In the Mississippi River, which has a large width and relatively low transverse mixing rate, β is small. In the Stony River, which has a small width and a high mixing rate, β is much larger. The quantity U/β is proportional to the length of the advective zone by a factor of $\alpha^*/12$. The values of U/β range several orders of magnitude and correlate to advective lengths of a few meters to several kilometers.

The effects of varying α and β are shown in Fig. 4.2. To simplify this analysis, only time series of concentration are considered. The tracer-response curves are presented in dimensional form because the effects of the parameters, especially β, would be difficult to discern in dimensionless form. Increasing α results in a decrease in peak concentration and an increase in the spread of the concentration distribution (Fig. 4.2a). This increase in dispersion is expected because the velocity gradients are larger when more of the channel is occupied by the stagnant zone. As Eq. 106 and 108 show, α affects neither the centroid μ_t nor (for large distances from the source) the skewness.

In some ways the effects of β are the opposite of the effects of α (Fig. 4.2b). Increasing β results in an increase in peak concentration, a decrease in the spread of the concentration distribution, a decrease in the skew of the concentration distribution, and little change of the centroid. These qualitative effects agree with Taylor's analysis. For a given tracer parcel, increasing transverse mixing (i.e., β given Eq. 56 and 63) increases the rate the parcel samples the velocity gradient, which decreases the differences in the individual parcels velocity from the mean parcel velocity; this, in turn, decreases the shear dispersion. The decrease in skew results from the decrease in the length of the advective zone as transverse mixing (i.e., β) increases.

Some of these conclusions are supported by Eq. 113, which relates α and β to the dispersion coefficient K. Eq. 18 shows that the peak concentration is proportional to $K^{-1/2}$ and the cloud width is proportional to $K^{1/2}$. Therefore, in terms of the parameters of the model of Reichert and Wanner (1991), the peak concentration is proportional to $\beta^{1/2}/\alpha$ and the cloud width is proportional to $\alpha/\beta^{1/2}$. These more quantitative relationships are illustrated in Fig.

4.2: The peak concentration is 3 times smaller for $\alpha = 0.3$ than for $\alpha = 0.1$, and it is smaller by a factor of $2^{1/2}$ for $\beta = 0.05$ than for $\beta = 0.1$. If the concentration was measured at a fixed time, t, the same relationships would hold for the spatial variance, skew, and arrival time.
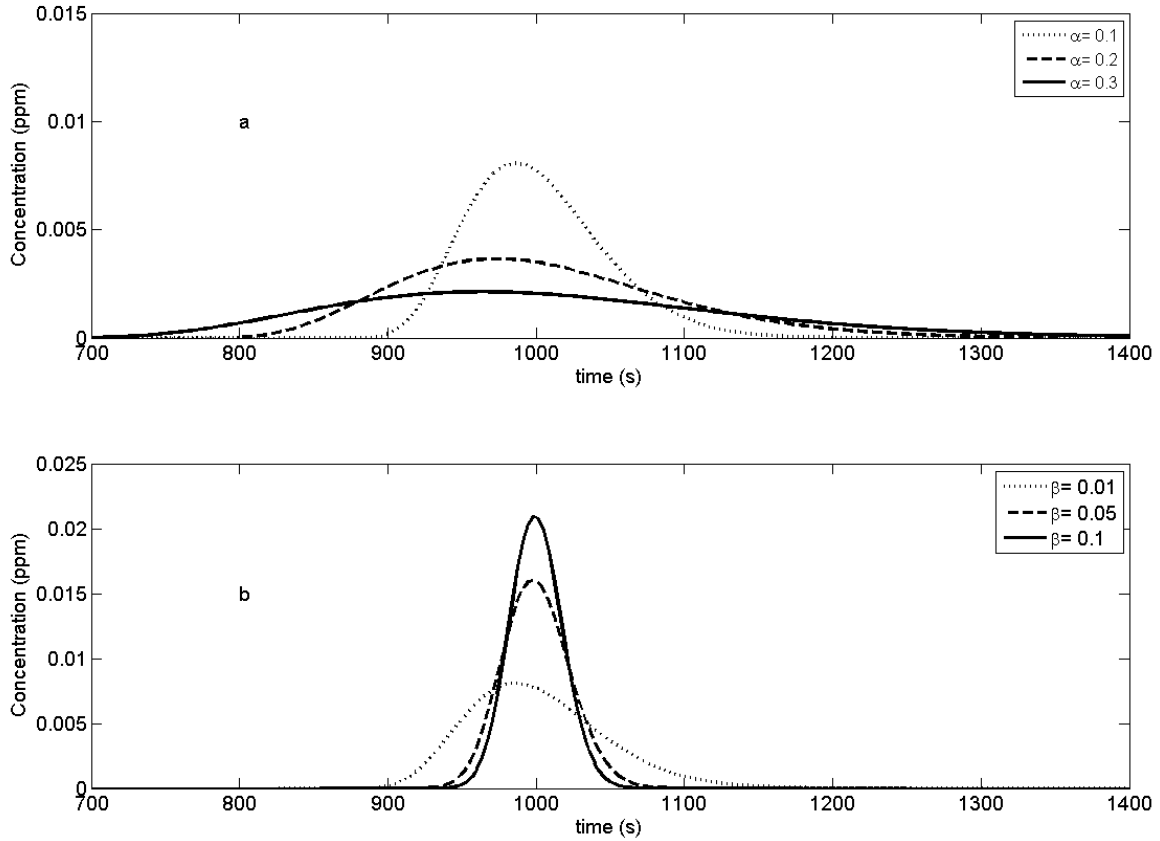
Figure 4.2: Effect of varying α and β. a. Varying α with $\beta = 0.01$ s^{-1} fixed. b. Varying β with $\alpha = 0.1$ fixed. The results are based on a hypothetical scenario in which 1 kg of tracer is injected as a Gaussian pulse in the center of the river with $\sigma_0 = 7.5$ m. The mean velocity equal to 0.1 m/s and the concentration is measured 500 m from the initial input. The length of the advective zone, L_x for of $\overline{U} = 0.1$ and $\beta = 0.01$ s^{-1} is 120m.

Behavior of the Moments

The spatial and temporal moments of the concentration distribution are analyzed to verify the analytical solution to the Reichert and Wanner model. Furthermore, the behavior of the moments verifies that the Reichert and Wanner model accurately describes dispersion processes, in and out of the advective zone, as described in Chapter 2.

Spatial Moments

Solutions for M, μ_x, σ_x^2, and γ_x are plotted with respect to t' (Fig. 4.3). Based on the expressions given by Eq. 98-102, the following behavior is expected: (1) M is constant for all time t; (2) μ_x grows linearly, and it is proportional to the mean velocity $\overline{U}$; (3) σ_x^2 is initially non-linear, but for $t' > 1$, its growth is linear; and (4) for $t' > 1$, the rate of growth in γ_x is negative. The time $t' = 1$ corresponds to the time required to travel through the advective zone. These behaviors, all observable in Fig. 4.3, agree with the dispersion processes described in Chapter 2, particularly regarding the rate of change in σ_x^2 and γ_x. In particular, the slope of the variance curve for large time is $2\alpha^2 U/\beta$, or twice the dispersion coefficient (Eq. 114). This result confirms the calculation of Reichert and Wanner (1991) using Fourier transforms and asymptotic analysis of the transport equations.

All three solutions to M and μ_x agree with each other, and the agreement between analytical solution and the numerical solution verifies that the expressions given by Eq. 98-102 are mathematically accurate. However, for σ_x^2, and γ_x the integrated solution diverges from the numerical and analytical solution. Calculating the concentration with Eq. 93 involves numerical integration; this results in some degree of numerical error.
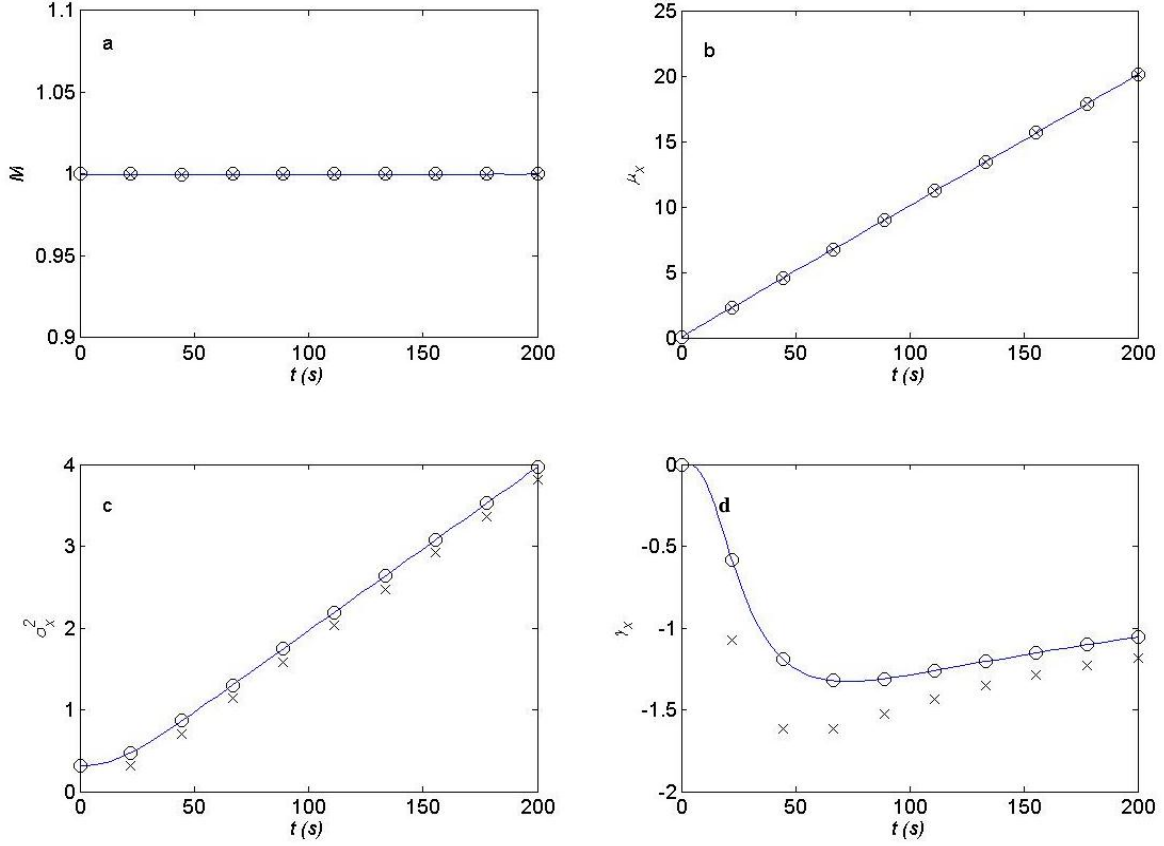
Figure 4.3: Evolution of the spatial parameters in time: (a) M_0 (kg), (b) center of mass (m), (c) variance (m^2),

and (d) skewness (m^3). Three different solutions are given: the analytical solution computed by Eq. 97-100

(solid line); the numerical solution computed by MATLAB (marked by 'o'); and the solution computed by

integrating the concentration curves calculated with Eq. 89 (marked with 'x'). All curves were calculated for M_0

$=1$ kg , $\alpha = 0.1$, $\beta = 0.01$ s^{-1}, $\overline{U} = 0.1$m/s and $\sigma_0 = 1/\sqrt{\pi}$ m.

Minimizing the error requires using small spatial steps, enough time steps to resolve

the convolutions accurately, and a large enough spatial range to compute the moments.

Nevertheless, the error in the centroid, variance, and skewness results from the small

difference of large numbers. Although the error for all four moments is less than 1.5% (Table

4.2), the error increases for the higher order moments, and the parameters σ_x^2 and γ_x, which

are computed with higher order moments, show pronounced error. The analytical and

numerical solutions have negligible differences and that is why they are given by a single value in Table 4.2

Table 4.2: Error in the first four spatial moments.

Time (s)	$\underline{M_{0x}}$ (kg)		$\underline{M_{1x}}$ (kg m)		$\underline{M_{2x}}$ (kg m^2)		$\underline{M_{3x}}$ (kg m^3)	
	Analytical and Numerical	Integrated	Analytical and Numerical	Integrated	Analytical and Numerical	Integrated	Analytical and Numerical	Integrated
22	1	1	2.32	2.31	5.84	5.67	15.60	14.40
44	1	1	4.54	4.54	21.54	21.35	105.00	102.50
66	1	1	6.77	6.76	47.13	46.93	335.30	331.10
88	1	1	8.99	8.98	82.58	82.38	771.40	766.00
111	1	1	11.21	11.21	127.94	127.71	1480.70	1473.30
133	1	1	13.43	13.43	183.10	182.92	2528.70	2518.60
155	1	0.99	15.65	15.65	248.24	248.00	3978.50	3967.80
177	1	0.99	17.87	17.57	323.15	322.96	5896.30	5886.80
200	1	0.99	20.10	20.10	407.98	407.79	8351.50	8341.40
Error (%)	--	**0.003**	--	**0.004**	--	**0.55**	--	**1.49**

The behavior of the first four spatial moments in each zones—F_{0x}, S_{0x}, F_{1x}, S_{1x}, F_{2x}, S_{2x}, F_{3x}, S_{3x}—provides additional insight in the movement and exchange of tracer as it travels downstream. The expressions for F_{nx} (B.25, B.26, B.39, and B.32) and S_{nx} (B.25, B.27, B.30, and B.33) as well as the relationships established in Eq. 20-22, are used to compute the solutions for the spatial parameters in each zone—M_{0f}, M_{0s}, μ_f, μ_s, σ_f^2, σ_s^2, γ_f and γ_s (Fig. 4.3). After an initial period, the masses in the two zones become equal and constant (Fig. 4.3a).

Figure 4.4: Evolution of the spatial parameters for the flowing zone and stagnant zone in dimensionless time, t': (a) M_0 (kg), (b) center of mass (m), (c) variance (m^2), and (d) skewness (m^3). Solid lines are the solutions for the flowing zone and dotted line are solutions for the stagnant zone. All curves were calculated for $M_i = 1$ kg, $\alpha = 0.1$, $\beta = 0.01$ s^{-1}, $\overline{U} = 0.1$ m/s and $\sigma_0 = 1/\sqrt{\pi}$ m.
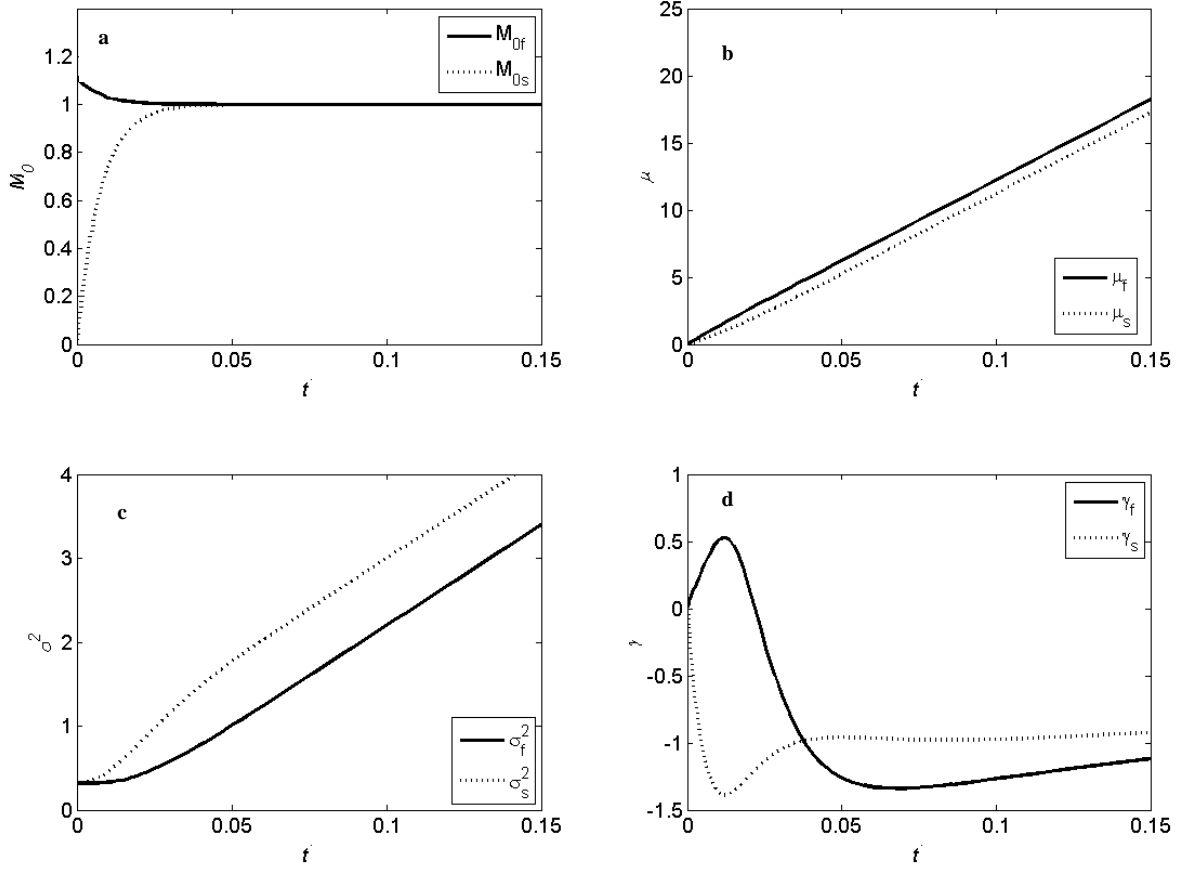
This duration of this period is defined as the equilibrium time, or t_{eq}; this parameter is given by the proportionality

$$t_{eq} \propto \frac{\alpha(1-\alpha)}{\beta} \tag{120}$$

The inverse of the proportionality index is a common term in the solution for C, C_1, and C_2. The center of mass is always greater in the flowing zone (Fig. 4.3b), and the variance is greater in the stagnant zone (Fig. 4.3c). The skewnesses for the two zones are equal to one

another approximately at t_{eq} (Fig. 4.3d). After t_{eq}, the skew in the two zones remains negative

and γ_s always exceeds γ_f; the skew in both zones approach zero. These relationships are

consistent with the spatial concentration curves given in Fig. 4.1 for the wider spike (solid

line). Because the curves were measured at $t' > 0.08$ the mass has already had sufficient time

to equilibrate between the two zones, and curves are past the zone of temporary positive

skew in the flowing zone.

Temporal Moments

The results from the temporal moment analysis can also be used to verify the

analytical solution. The solutions for M_t, μ_t, σ_t^2, and g_t from the analytical approximation

given by Eq. 101-104 (solid line) and the values obtained through the integration of the

concentration curve calculated with Eq. 93 (marked with 'x') are given in Fig 4.4; both

solutions agree well. Although the zeroth spatial moment is constant with respect to time, the

zeroth temporal moment varies close to the source because of the initial condition. At $x=0$,

M_{0t} only recognizes half of the initial Gaussian pulse, and therefore, the $M_{0t}(0) = 0.5$ kg-

s/m^3. After $x \approx 2\sigma_0$, the total mass has passed and M_{0t} is 1 kg-s/m^3. If the initial injection

were in the form of a spike M_{0t} would be constant for all x. For μ_t, σ_t^2, and g_t the

approximate form is linear with respect to x, and the computed results match well with the

theoretical predictions (Fig. 4.4b-d). Reichert and Wanner (1991) showed a delayed increase

in the variance for their results (Fig. 4 of Reichert and Wanner, 1991); we observe a delayed

increase in the spatial variance (Fig. 4.3b) but not the temporal variance.
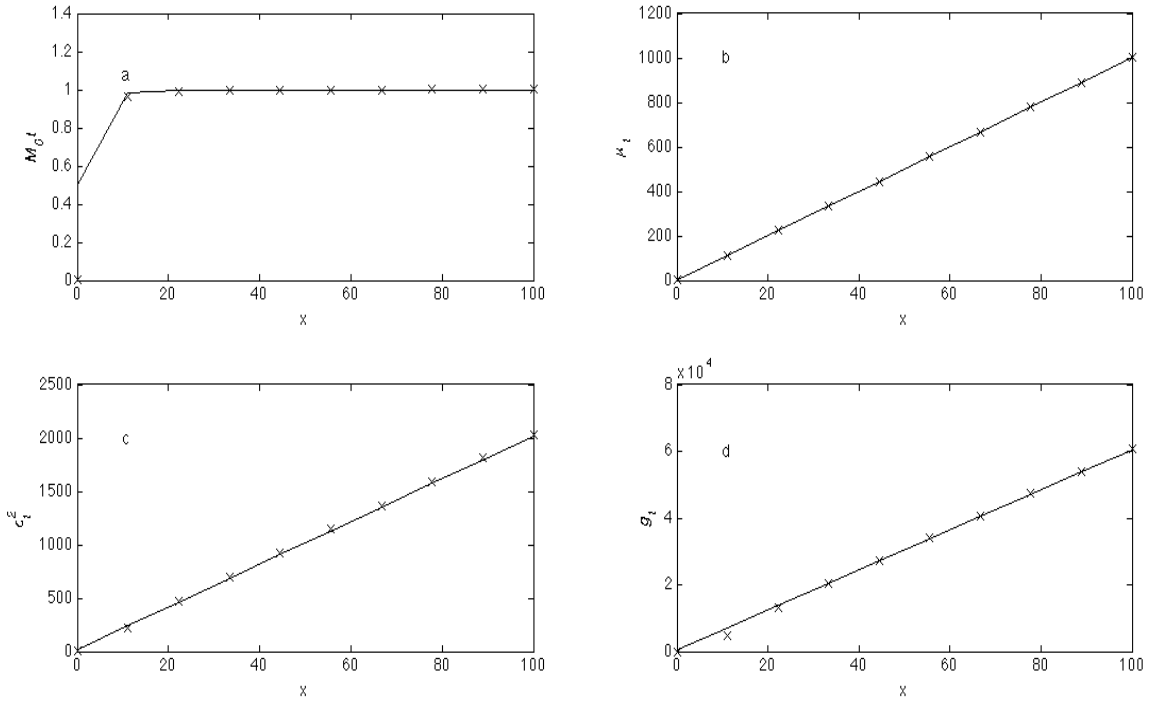
Figure 4.5: Evolution of the temporal moments in space: (a) M_{0t} (kg-s/m^3) (b) center of mass, (s), (c) variance, (s^2), and (d) skewness (s^3). Two different solutions are given: the analytical solution computed by Eq. 101-104 (solid line); and the solution computed through the integration of the concentration curve calculated with Eq. 89 (marked with 'x') All curves were calculated for M$_i$ = 1 kg, α = 0.1, β = 0.01 s^{-1}, $\overline{U}$ = 0.1 m/s and σ_0 = 7.5 m.

Comparison to Measured Results

The digitized measured results from Day's analysis were plotted against the predicted

results from this analysis (referred to as RW results), as well as Taylor's predicted results for

two different conditions: constant coefficient and optimized coefficient. The constant

Table 4.3: Parameter values for the Reichert and Wanner and Taylor Model

x (m)	U (m/s)	α (−)	β (1/s)	C_0 (ppm)	K (m^2/s)	M (mg)
Constant Coefficient Values						
All x	0.62	0.13	5.2×10^{-3}	6.9×10^2	1.2	9.2×10^3
Optimized Values						
50	0.94	0.04	5.7×10^{-3}	1.0×10^3	2.2×10^{-1}	1.4×10^4
62.5	0.86	0.17	3.7×10^{-2}	9.0×10^2	5.9×10^{-1}	1.2×10^4
75	0.86	0.46	2.1×10^{-1}	1.3×10^3	7.3×10^{-1}	1.7×10^4
87.5	0.84	0.23	3.4×10^{-2}	1.0×10^3	1.1	1.4×10^4
100	0.86	0.19	2.4×10^{-2}	1.0×10^3	1.1	1.4×10^4
125	0.73	0.21	7.5×10^{-3}	1.1×10^3	3.1	1.4×10^4
175	0.74	0.26	2.4×10^{-2}	9.6×10^2	1.6	1.3×10^4
200	0.77	0.18	9.6×10^{-3}	8.3×10^2	2.0	1.1×10^4
225	0.71	0.22	1.4×10^{-2}	1.1×10^3	1.8	1.4×10^4
250	0.68	0.23	1.3×10^{-2}	1.0×10^3	2.0	1.4×10^4
275	0.70	0.18	1.2×10^{-2}	6.4×10^2	1.3	8.6×10^3
300	0.70	0.32	3.5×10^{-2}	7.5×10^2	1.4	1.0×10^4
350	0.67	0.18	6.7×10^{-3}	9.4×10^2	2.1	1.2×10^4
400	0.66	0.40	5.5×10^{-2}	9.3×10^2	1.3	1.2×10^4
450	0.63	0.18	5.2×10^{-3}	9.1×10^2	2.3	1.2×10^4
500	0.65	0.13	5.2×10^{-3}	6.2×10^2	1.4	8.2×10^3

coefficient and optimized values for $\overline{U}$, α, β, C_0, and M, predicted from the moment

matching analysis described in Chapter 3 are given in Table 4.3. The channel area—a

parameter required for the models—was set at 0.76 m^2 based on the dimensions given by

Day (1975) and Day and Wood (1976). The advective length, L_x, for Thomas Reach is

estimated from the constant coefficient values of β and $\overline{U}$ and Fischer's coefficient of $\alpha^* =$ 0.4 to be approximately 570 m; therefore, all 16 measurements recorded by Day are within the advective zone.

Representative results for the constant coefficient and the optimized coefficient analysis are given in Fig. 4.5. The peak concentration, C_p, plotted as a function of the time of peak, t_p, for all five cases is given in Fig. 4.6. Finally, the ratios for the measured and predicted values of C_p, t_p, M, μ_t, σ_t^2 and g_t were computed for each sub-reach and plotted in Fig. 4.7.

Constant Coefficient Analysis

The tracer-response curves from the constant coefficient RW analyses arrive late compared to the measured data, but the timing improves as x increases because the velocity for the constant coefficient analysis is closer to the optimized velocity downstream. This point is illustrated in Fig. 4.6b; for $x' < 0.08$, the ratio of measured and predicted values of μ is ~0.7; at $x' = 0.2$, it is ~0.9; and farther downstream it is ~1. The curves for the constant coefficient RW results are roughly the same shape as the measured results, but this qualitative assessment is not apparent in the ratios of M, μ_t, σ_t^2 and g_t because Taylor's results produce just as good, if not better, predictions (Fig. 4.6a-d). However, the constant coefficient RW results predict C_p and t_p better than Taylor's results, especially for small x'. The average error for predicting the C_p and t_p for the two constant coefficient models is given in Table 4.4. The larger error for the time of arrival of the peak concentration is expected because of the error in predicting μ_t, the time of arrival of the center of mass.

Table 4.4: Average error for C_p and t_p for RW and Taylor results

	C_p Error (%)	t_p Error (%)
RW CC	3.1	15.8
RW OPT	9.9	0.1
Taylor CC	30.1	28.4
Taylor OPT	16.2	5.2

*CC- constant coefficient; *OPT- optimized coefficient

Optimized Coefficient Analysis

For most values of x', the optimized RW results fit the measured concentration curves much better than the constant coefficient RW and Taylor results, and for most cases, the optimized Taylor results. However, for small values of x', the optimized RW results overpredict σ_t^2 and underpredict C_p until approximately $x' = 0.15$. Reichert and Wanner (1991) also observed this behavior for small x' in their results, although the behavior went away by $x' = 0.08$. The ratios for M, $\mu_{t,}$, and $g_{t,}$ from the optimized RW results are approximately unity for all 16 locations. Taylor's optimized results are also approximately unity; however, the optimized RW results are better predicting C_p and t_p than Taylor's optimized results (Table 4.4).
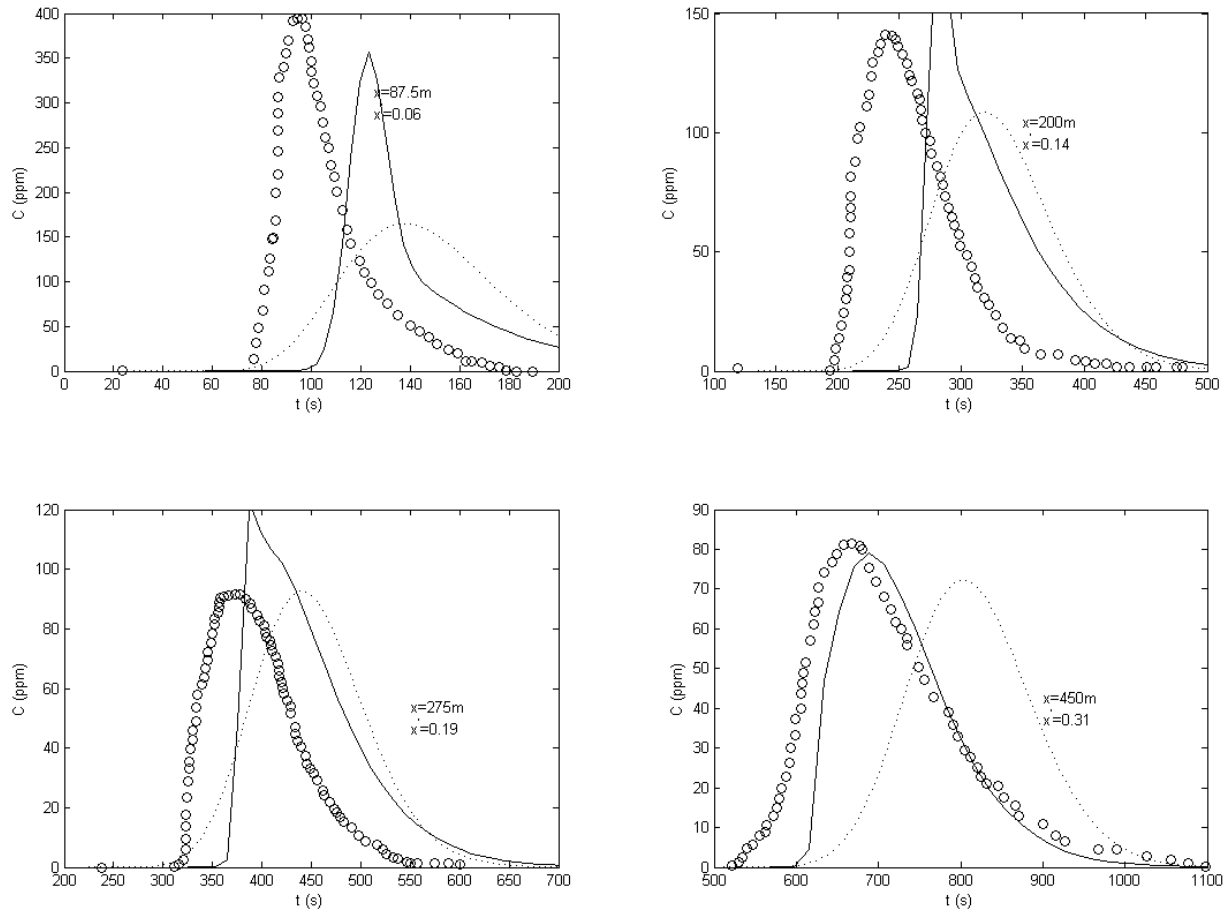
Figure 4.6: Predicted and measured results for the constant coefficient method for x = 87.5, 200, 275 and 450 m. Measured results given by 'o'; the predicted results from this analysis given by solid line and the predicted results from Taylor's analysis given by dotted line
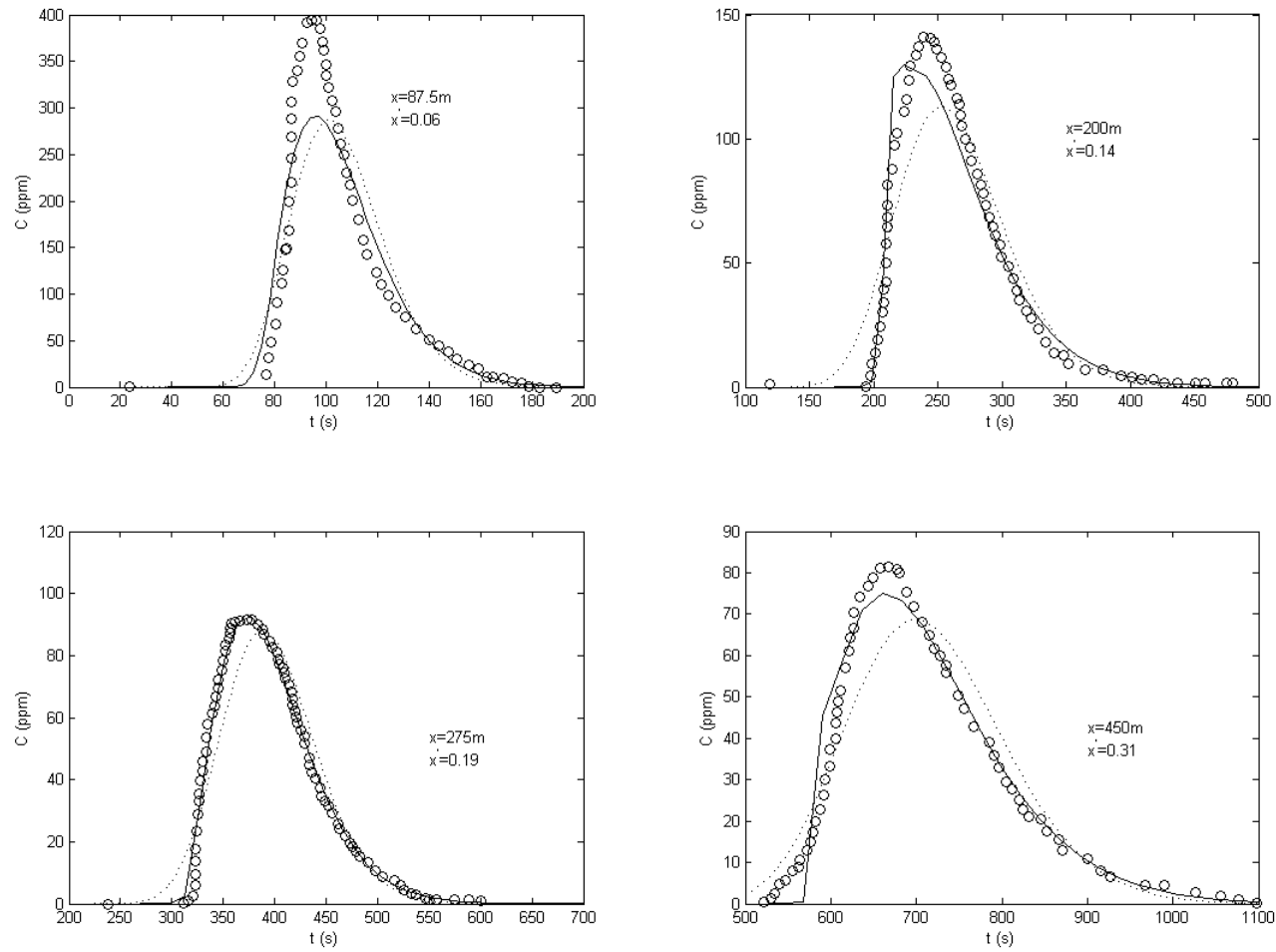
Figure 4.7: Predicted and measured results for the optimized coefficient method for x = 87.5, 200, 275 and 450 m. Measured results given by 'o'; the predicted results from this analysis given by solid line and the predicted results from Taylor's analysis given by dotted line.
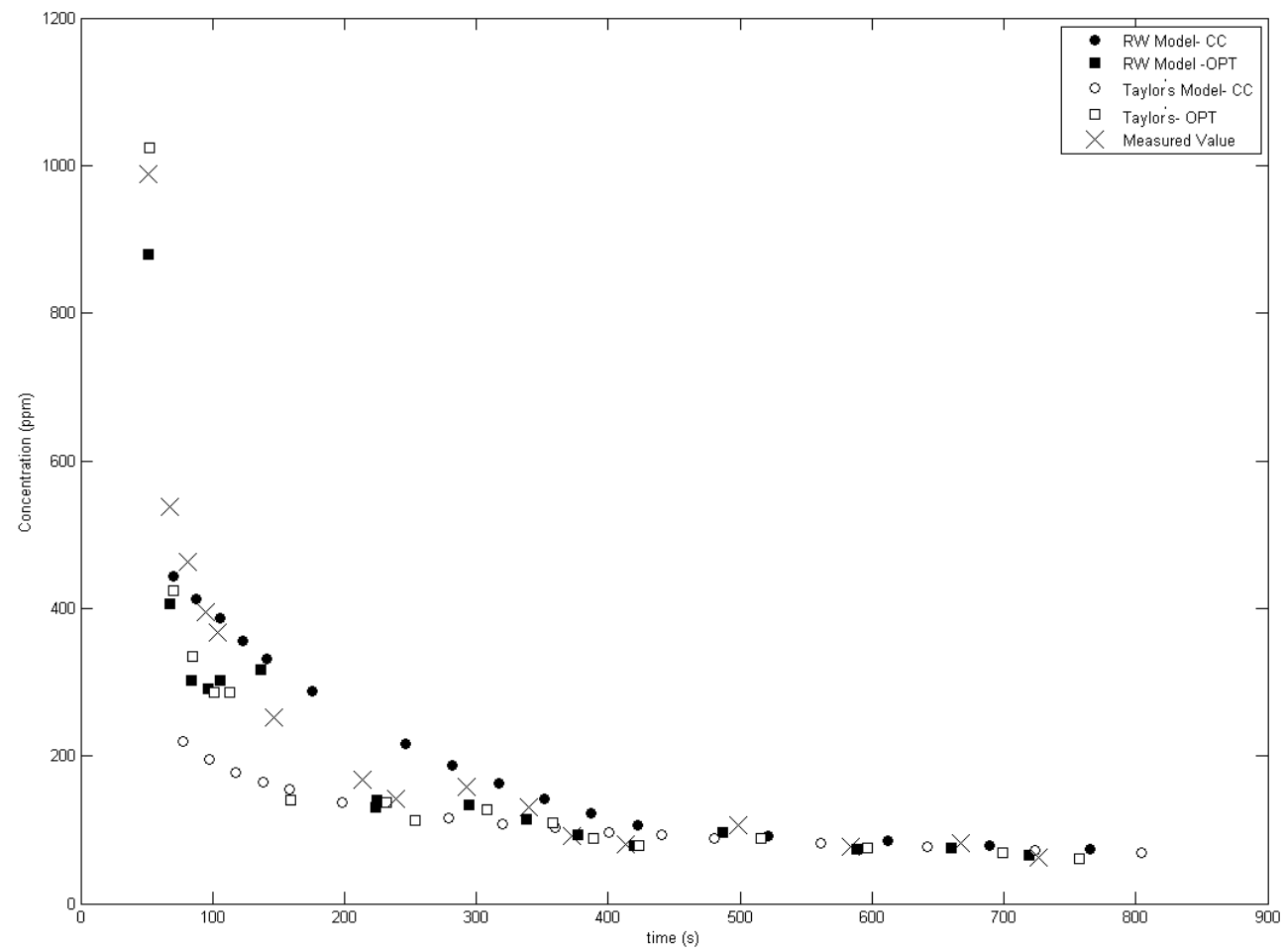
Figure 4.8: Measured and predicted peak for C_p plotted with respect to t_p.
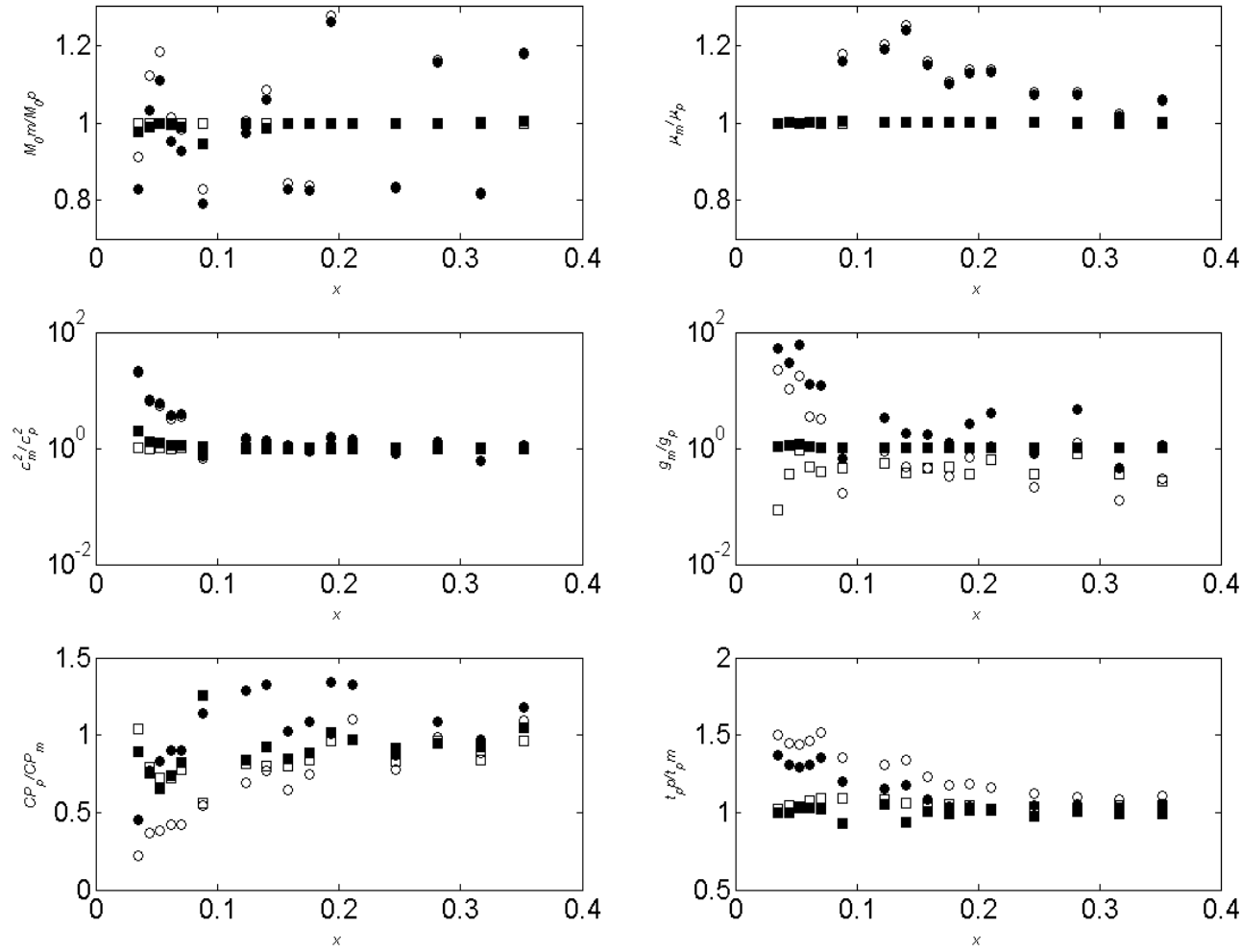
Figure 4.9: Ratio of measured vs. predicted values for M, μ_t, σ_t^2, g_t, C_p, and t_p: '●' represents ratios for constant coefficient values from this analysis; '■' represents ratios for optimized values from this analysis. Corresponding open circle and squares are the ratios computed from results from Taylor's analysis.

Model Assessment

The analytical solution to the Reichert and Wanner model is a verified solution to describe transport in the advective zone. This solution is useful for water quality engineers and scientists for modeling and predicting transport of contaminants or nutrients because the advective zone in rivers can be several kilometers long (Table 4.1). The analytical solution applies for distances outside the advective zone as well. After the advective length, the variance of the concentration distribution grows linearly at the rate predicted by Reichert and Wanner (1991). This agrees with Taylor's analysis, as well as several field study results. However, as with Taylor's model and the dead zone model, the skew of the concentration distribution predicted with the analytical solution goes to zero. Field tests in natural rivers do not verify that this actually happens (Schmid, 2002).

The solution requires very little in terms of input, especially when compared with alternative advective zone models, such as the two-dimensional streamtube model. The model parameters, α and β, can be empirically estimated from the equations given by Reichert and Wanner (1991), or computed from the moments of tracer response curves as done in this analysis. This study illustrates the effect of varying α and β and provides a simple physical explanation for their effects on conservation curves. Applied to the data of Day (1975), the model reproduces the tracer response curves better than Taylor model, especially in predicting the peak concentration and arrival time (Table 4.3). The application with constant values of α and β performed better in predicting the peak concentration of measured results than the application with values optimized to reproduce the first four moments at the measured locations. This performance is encouraging because the constant-

coefficient model can be applied with only limited field data.   However, the constant coefficient model underpredicted the arrival time of the tracer cloud. If more velocity measurements were available, the approximation of $\overline{U}$ would likely be more representative of field conditions and the timing of the predicted curve would likely improve.

Because the solution is analytical, it avoids the spurious diffusion produced by numerical approximation. However, the solution requires the numerical evaluation of a convolution integral. Effects of the numerical precision are apparent for variance and skewness which involve small differences in large numbers. Additionally, the analytical solution includes a term that produces a spike in the predicted concentration curves if the initial pulse is too narrow. When this is the case, the initial pulse remains in the flowing zone until the mass of the pulse has had sufficient time to equilibrate between the two zones. A spike is present in the predicted concentration curves for C and C_1 until this equilibrium occurs (approximately at $x' = 0.2$). Reichert and Wanner (1991) also observed this in their results. For a sufficiently wide pulse ($\psi > 1.5$), the spike is not present in the results.

CHAPTER 5: CONCLUSIONS

Summary

Transport within the advective zone cannot be accurately modeled with available one-dimensional solutions, such as Taylor's, because they apply only after a balance between longitudinal advection and transverse dispersion has been reached. Two-dimensional advective-zone solutions apply within the advective zone but require extensive input from the user. The purpose of this research was to obtain and verify an analytical solution to a one-dimensional model that applies within the advective zone. The model used was devised by Reichert and Wanner (1991) and involves two parameters: the fraction of the channel occupied by the stagnant zone and a transfer coefficient. These parameters can be estimated from empirical equations or a moment-matching scheme. The later requires tracer response curves but results in parameters that are more representative of channel conditions.

The solution to the model was derived through the application of an iterative Laplace transform given by Sneddon (1972). De Smedt (2005) outlined a procedure that used the iterative Laplace transform to obtain an analytical solution to the dead zone model; because the transport equations to the dead zone model are mathematically similar, this procedure was followed closely to obtain the analytical solution to the Reichert and Wanner model. The solution, given by Eq. 93, requires numerical integration of the convolution integral. It can be used to calculate concentration as a function of x or t. The solution was verified through an analysis of the temporal and spatial moments. The moments to the Reichert and Wanner model are not available in current literature so analytical expressions were obtained by solving a set of ODEs with specified boundary conditions (for the spatial case) and with

Laplace transforms (for the temporal case). Numerical solutions for the spatial moments were also computed in Matlab; this provided verification that the solutions for the analytical spatial moments were correct. The results from the moment analysis verified the analytical solution to the Reichert and Wanner model.

The model was applied to measurements from a tracer study conducted by Day (1975) in a mountain stream. Several measuring locations were within the advective zone. Tracer concentration curves, channel geometry, and hydrologic conditions for the stream were presented in Day (1975), Day (1976) and Day and Wood (1976). The concentration curves published in Day and Wood (1976) were digitized so the results could be compared with the curves predicted from our solution. Concentration curves predicted with Taylor's solution were also computed to see how well it compares to the measured data and to our model. Our solution reproduced the tracer response curves better than Taylor's model, especially in predicting the peak concentration and arrival time. The predicted results would likely improve with additional field data, but it is encouraging to know that it performs better than available solutions given limited data.

Recommendations and Future Work

The impact of this work would be strengthened if the results from this solution could be compared with results from a dye study conducted in a meandering channel, such as the South Skunk River. A meandering channel will likely have much different value for α and β, and it would be interesting to see if the solution would perform as well, if not better, given the different channel conditions. We would hope to conduct the dye study ourselves, or at least work with those conducting the dye study, so the necessary field data could be

measured. Additionally, a numerical solution of this model would be useful and would serve

as an alternative to this solution when channel conditions cannot be modeled with a single

parameter. Finally, additional analytical solutions could be obtained for different initial

conditions and boundary conditions (e.g., maintained source and injection within the stagnant

zone).

APPENDIX A: MATLAB FUNCTIONS

This research required the use of MATLAB to compute the results presented in Chapter 4. Below is a list of the MATLAB codes used to compute results. The corresponding codes are presented on the following pages.

MATLAB Function Files

Function 1: *Cvst.m*: The analytical solution to the RW model with respect to time

Function 2: *Cvsx.m:* The analytical solution to the RW model with respect to space

Function 3: *an_moments.m*: The analytical solutions to the spatial moments

Function 4: *num_mom_func.m*: Generates the set of ODEs for *num_moments.m* to solve

Function 5: *num_moments.m*: The numerical solutions to the spatial moments

Function 6: *temp_moments.m*: The analytical approximation to the temporal moments

Function 1

```matlab
%Name:    Cvst.m


%Purpose: Solves the analytical solution to the Reichert and Wanner model
%with respect to time for a given locaiton x (for this case, x=100).



clear; close all



  %Set constants
  x     = 100;
  M0    = 1;                    %  Source concentration (mg/L)
  sig   = 0.5;                  %  Parameter describing the spread of the
initial pulse (m)
  U     = 0.5;                  %  Mean velocity (m/s)
  A     = 1;                    %  Cross-sectional area (m2) (est. from Day)
  K     = 1;                    %  Dispersion coefficient (m2/s)
  alpha = 0.1;                  %  Fraction of channel in stagnant zone
  bta   = 0.01;                 %  Model coefficient
  nt    = 100;                  %  Number of points in t
  ntau  = 1000;                 %  Number of points for integrand in
convolution integral
  tf1   = 0.1;                  %  Factor for the start of the time range
  tf2   = 3;                    %  Factor for the end of the time range
  tauf  = 1e-5;                 %  Parameter used to avoid singularities in
calculations
  C0    =(M0*U)/(sqrt(pi)*sig*(1-alpha)); %Initial Concentration


  %  Plot the initial condition

  xinit = sig*linspace(-4,4);
  Cinit = C0*exp(-xinit.^2/sig^2);



%  Set up time range

  ta = x*(1-alpha)/U;
  t  = ta*linspace (tf1,tf2,nt)';          %  Time (sec)

%  Compute concentration in the flowing zone

  term11 = exp (-(x-U*t/(1-alpha)).^2/sig^2).*exp(-bta*t/(1-alpha));
  term12 = NaN*ones(nt,1);
  for i = 1:length(t)
     tau       = t(i)*linspace(tauf,1-tauf,ntau);
     F1        = exp(-(x-U*tau/(1-alpha)).^2/sig^2);
     F2        = exp(-bta*tau/(1-alpha));
     F3        = exp(-bta*(t(i)-tau)/alpha);
     F4        = sqrt(bta^2*tau./(alpha*(1-alpha)*(t(i)-tau)));
```

```matlab
        F5          = besseli(1,2*sqrt(bta^2*tau.*(t(i)-tau)/(alpha*(1-
alpha)))));
        term12(i) = trapz(tau,F1.*F2.*F3.*F4.*F5);
    end
    C1 = C0*(term11 + term12);

%  Compute concentrations in the stagnant zone

    term21 = NaN*ones(nt,1);


    term22 = NaN*ones(nt,1);
    for i = 1:length(t)
        tau         = t(i)*linspace(tauf,1-tauf,ntau);
        F1          = exp(-(x-U*(t(i)-tau)/(1-alpha)).^2/sig^2);
        F2          = exp(-bta*(t(i)-tau)/(1-alpha));
        F3          = exp(-bta*tau/alpha);
        term21(i) = (bta/alpha)*trapz(tau,F1.*F2.*F3);
    end

    for i = 1:nt
        tau2        = t(i)*linspace (tauf,1-tauf,ntau)';
        F1          = exp(-bta*tau2/alpha);
        F2          = NaN*ones(ntau,1);
        for j = 1:ntau
            tau1    = (t(i)-tau2(j))*linspace(tauf,1-tauf,ntau);
            G1      = exp(-(x-U*tau1/(1-alpha)).^2/sig^2);
            G2      = exp(-bta*tau1/(1-alpha));
            G3      = exp(-bta*(t(i)-tau2(j)-tau1)/alpha);
            G4      = sqrt(bta^2*tau1./(alpha*(1-alpha)*(t(i)-tau2(j)-tau1)));
            G5      = besseli(1,2*sqrt(bta^2*tau1.*(t(i)-tau2(j)-
tau1)/(alpha*(1-alpha)))));
            F2(j) = trapz(tau1,G1.*G2.*G3.*G4.*G5);
        end
        term22(i) = trapz(tau2,F1.*F2);
    end

    C2 = (C0*bta/alpha)*(term21+term22);

    C= (1-alpha)*C1+alpha*C2;


    figure (1); plot (t, C)
```

Function 2

```
%Name:     Cvsx.m

%Purpose: Solves the analytical solution to the Reichert and Wanner model
%with respect to space for a given time t after injection(for this case,
%t=100).



   clear; close all

%  Set constants

   M      =1;
   t      = 100;
   sig    = 1;                  %  Parameter describing the spread of the
initial pulse (m)
   U      = 0.5;                %  Mean velocity (m/s)
   A      = 1;                  %  Cross-sectional area (m2) (est. from Day)
   K      = 1;                  %  Dispersion coefficient (m2/s)
   alpha = 0.2;                 %  Fraction of channel in stagnant zone
   bta   = 0.01;                %  Model coefficient
   nx    = 100;                 %  Number of points in t
   ntau  = 1000;                %  Number of points for integrand in
convolution integral
   xf1   = 0.1;                 %  Factor for the start of the time range
   xf2   = 2;                   %  Factor for the end of the time range
   tauf  = 1e-5;                %  Parameter used to avoid singularities in
calculations
   C0     = (M*U)/(sig*sqrt(pi));          %  Source concentration (mg/L
   x0     = 2;                  %  Injection site (m)

%  Compute initial mass

   xinit = sig*linspace(-8,8);
   Cinit = C0*exp(-(xinit-x0).^2/sig^2);
   M0    = (1-alpha)*trapz(xinit,Cinit);              %  (1-alpha)
accounts for the injection in the flowing zone

%  Set up spatial coordinate

   xp = x0+U*t/(1-alpha);
   x  = xp*linspace(xf1,xf2,nx)';       %  Distance (m)

%  Compute concentration in the flowing zone

   term11 = exp(-(x-x0-U*t/(1-alpha)).^2/sig^2)*exp(-bta*t/(1-alpha));

   tau = t*linspace(0,1-tauf,ntau);
   F2  = exp(-bta*tau/(1-alpha));
   F3  = exp(-bta*(t-tau)/alpha);
```

```matlab
    F4   = sqrt(bta^2*tau./(alpha*(1-alpha)*(t-tau)));
    F5   = besseli(1,2*sqrt(bta^2*tau.*(t-tau)/(alpha*(1-alpha))));

    term12 = NaN*ones(nx,1);
    for i = 1:nx
        F1       = exp(-(x(i)-x0-U*tau/(1-alpha)).^2/sig^2);
        term12(i) = trapz(tau,F1.*F2.*F3.*F4.*F5);
    end

    C1 = C0*(term11 + term12);


% Compute concentrations in the stagnant zone

    term21 = NaN*ones(nx,1);
    term22 = NaN*ones(nx,1);

    tau = linspace(0,t,ntau);
    F2  = exp(-bta*(t-tau)/(1-alpha));
    F3  = exp(-bta*tau/alpha);

    for i = 1:length(x)
        F1       = exp(-(x(i)-x0-U*(t-tau)/(1-alpha)).^2/sig^2);
        term21(i) = trapz(tau,F1.*F2.*F3);
    end

    for i = 1:nx
        tau2     = t*linspace(0,1-tauf,ntau)';
        F1       = exp(-bta*tau2/alpha);
        F2       = NaN*ones(ntau,1);
        for j = 1:ntau
            tau1  = (t-tau2(j))*linspace(tauf,1-tauf,ntau);
            G1    = exp(-(x(i)-x0-U*tau1/(1-alpha)).^2/sig^2);
            G2    = exp(-bta*tau1/(1-alpha));
            G3    = exp(-bta*(t-tau2(j)-tau1)/alpha);
            G4    = sqrt(bta^2*tau1./(alpha*(1-alpha)*(t-tau2(j)-tau1)));
            G5    = besseli(1,2*sqrt(bta^2*tau1.*(t-tau2(j)-tau1)/(alpha*(1-
alpha))));
            F2(j) = trapz(tau1,G1.*G2.*G3.*G4.*G5);
        end
        term22(i) = trapz(tau2,F1.*F2);
    end


    C2 = C0*(bta/alpha)*(term21+term22);
    C = (1-alpha)*C1 + alpha*C2;

 figure (1); plot (x, C)
```

Function 3

```matlab
%Name:     an_moments.m

%Purpose: Solves the analytical expressions for the spatial moements


clear; close all

a=0.1;
U=0.1;
b=0.01;
M=1;
s=1/sqrt(pi);


 %Calc the Analytical Solutions


l=exp((b*t)/(a*(-1+a)));

U1= -((-a+a*exp((b*t)/(a*(-1+a)))+1)*M)/(-1+a);

U2= -(-1+exp((b*t)/(a*(-1+a))))*M;

U3= -((2*a^4*exp((b*t)/(a*(-1+a)))-2*a^4-4*a^3*exp((b*t)/(a*(-1+a)))...
+4*a^3-a^2*b*t.*exp((b*t)/(a*(-1+a)))-2*a^2+2*a^2*exp((b*t)/(a*(-1+a)))...
-b*t*a^2+2*b*t*a-b*t)*M*U)/(b*(-1+a)^2);

U4= -((2*a^3*exp((b*t)/(a*(-1+a)))-2*a^3+3*a^2-3*a^2*exp((b*t)/(a*(-
1+a)))...
-b*t*a-a*b*t.*exp((b*t)/(a*(-1+a)))-a+a*exp((b*t)/(a*(-1+a)))...
+b*t)*M*U)/(b*(-1+a));

U5= -(1/(b^2*(-1+a)*(-2*a+a^2+1)))...
*((-54*a^5*U^2+6*l*a^3*U^2-42*l*a^6*U^2+12*a^4*U^2*l.*t.*b...
-6*a^3*U^2*l.*t.*b-3*s^2*b^2*a-s^2*b^2*a^3+3*s^2*b^2*a^2+30*a^4*U^2...
+s^2*b^2*30-6*a^3*U^2-6*a^5*U^2*l.*t.*b+a^3*U^2*l.*t.^2*b^2-
18*a^3*U^2*t*b...
+18*a^4*U^2*t*b-
6*a^5*U^2*t*b+6*a^2*U^2*t*b+U^2*t.^2*b^2+3*U^2*t.^2*b^2*a^2...
-U^2*t.^2*b^2*a^3-3*U^2*t.^2*b^2*a+42*a^6*U^2-12*a^7*U^2+l*s^2*b^2*a...
-2*l*s^2*b^2*a^2+l*s^2*b^2*a^3+54*l*a^5*U^2+12*l*a^7*U^2-30*l*a^4*U^2)*M);

U6 = -(1/((-1+a)^2*b^2))*((-b^2*U^2*t.^2-
b^2*U^2*t.^2*a^2+2*b^2*U^2*t.^2*a...
-36*a^5*U^2*l-s^2*b^2+16*a^3*U^2-2*a^2*U^2-38*a^4*U^2-2*a*l.*s^2*b^2...
+a^2*l.*s^2*b^2+36*a^5*U^2-12*a^6*U^2-6*a^4*U^2*b*l.*t+l.*s^2*b^2...
+2*s^2*b^2*a-s^2*b^2*a^2+2*l.*a^2*U^2-10*b*a^2*U^2*t+14*b*a^3*U^2*t...
-6*b*a^4*U^2*t-4*a^2*U^2*l.*t.*b+a^2*U^2*l.*t.^2*b^2+2*b*a*U^2*t...
+12*a^6*U^2*l+38*a^4*U^2*l-16*a^3*U^2*l+10*a^3*U^2*b*l.*t)*M);

U7 = -U*M*(-120*a^10*U^2-600*a^9*exp(b*t/(a*(-1+a)))...
```

```
*U^2-24*exp(b*t/(a*(-1+a)))*b^2*s^2*a^3-12*b^2*U^2*t.^2*a^6...
-12*b^2*U^2*t.^2*a^2+48*b^2*U^2*t.^2*a^5-72*b^2*U^2*t.^2*a^4...
-60*b*a^8*U^2*t-156*b*a^4*U^2*t+264*b*a^7*U^2*t+600*a^9*U^2...
-24*a^4*U^2-456*b*a^6*U^2*t+24*b*a^3*U^2*t+48*b^2*U^2*t.^2*a^3...
+1224*a^8*exp(b*t/(a*(-1+a)))*U^2+744*a^6*exp(b*t/(a*(-1+a)))...
*U^2+120*a^10*exp(b*t/(a*(-1+a)))*U^2+6*exp(b*t/(a*(-1+a)))...
*b^2*s^2*a^2+384*b*a^5*U^2*t-60*a^8*U^2*b*l.*t-a^4*U^2*b^3*l.*t.^3...
+12*a^6*U^2*b^2*l.*t.^2-1224*a^8*U^2+1296*a^7*U^2-U^2*t.^3*b^3*a^4...
-216*a^5*exp(b*t/(a*(-1+a)))*U^2+24*a^4*exp(b*t/(a*(-1+a)))*U^2...
+216*a^5*U^2-744*a^6*U^2-U^2*t.^3*b^3+4*U^2*t.^3*b^3*a+4*U^2*t.^3*b^3...
*a^3-6*U^2*t.^3*b^3*a^2-36*a^4*U^2*b*l.*t-36*b^2*s^2*a^4+24*b^2*s^2*a^3...
-6*b^2*s^2*a^2+6*a^3*l.*t.*b^3*s^2-3*a^2*l.*t.*b^3*s^2-
3*a^4*l.*t.*b^3*s^2...
-1296*a^7*l.*U^2-24*l.*b^2*s^2*a^5+36*l.*b^2*s^2*a^4+6*a^6*l.*b^2*s^2...
-288*a^6*U^2*b*l.*t+216*a^7*U^2*b*l.*t+168*a^5*U^2*b*l.*t-
24*a^5*U^2*b^2...
*l.*t.^2+12*a^4*U^2*b^2*l.*t.^2+24*b^2*s^2*a^5-6*b^2*s^2*a^6-
3*b^3*t.*s^2...
+12*b^3*t.*a*s^2-3*b^3*t.*s^2*a^4+12*b^3*t.*s^2*a^3-18*b^3*t.*s^2*a^2)...
/((-3*a^2+a^3+3*a-1)*(-1+a)*b^3);


U8 = -U*M*(120*a^9*l.*U^2+27*l.*b^2*s^2*a^3-3*b^2*U^2*t.^2*a...
+21*b^2*U^2*t.^2*a^2-
12*b^2*U^2*t.^2*a^5+39*b^2*U^2*t.^2*a^4+222*b*a^4*U^2*t...
-60*b*a^7*U^2*t-120*a^9*U^2+90*a^4*U^2-6*a^3*U^2+228*b*a^6*U^2*t...
-66*b*a^3*U^2*t-45*b^2*U^2*t.^2*a^3-540*a^8*l.*U^2-882*a^6*l.*U^2-
15*l.*b^2*s^2*a^2...
+3*l.*a*b^2*s^2-330*b*a^5*U^2*t+540*a^8*U^2-972*a^7*U^2-a^3*U^2*l.*t.^3...
*b^3+6*b*a^2*U^2*t+414*a^5*l.*U^2-90*a^4*l.*U^2+6*a^3*l.*U^2-
3*a*l.*t.*b^3...
*s^2-414*a^5*U^2+882*a^6*U^2+U^2*t.^3*b^3-3*U^2*t.^3*b^3*a-
U^2*t.^3*b^3*a^3+3...
*U^2*t.^3*b^3*a^2-3*a*b^2*s^2+108*a^4*U^2*b*l.*t-18*a^3*U^2*b*l.*t...
+21*b^2*s^2*a^4-27*b^2*s^2*a^3+15*b^2*s^2*a^2-3*a^3*l.*t.*b^3*s^2...
+6*a^2*l.*t.*b^3*s^2+972*a^7*l.*U^2+6*l.*b^2*s^2*a^5-21*l.*b^2*s^2*a^4...
+192*a^6*U^2*b*l.*t-60*a^7*U^2*b*l.*t-
222*a^5*U^2*b*l.*t+12*a^5*U^2*b^2*l.*t.^2...
+9*a^3*U^2*b^2*l.*t.^2-21*a^4*U^2*b^2*l.*t.^2-
6*b^2*s^2*a^5+3*b^3*t.*s^2...
-9*b^3*t.*a*s^2-3*b^3*t.*s^2*a^3+9*b^3*t.*s^2*a^2)/((-3*a^2+a^3+3*a-
1)*b^3);




M0_a = (1-a)*U1+a*U2;
M1_a = (1-a)*U3+a*U4;
M2_a = (1-a)*U5+a*U6;
M3_a = (1-a)*U7+a*U8;
mu_a = M1_a./M0_a;
var_a = M2_a./M0_a - mu_a.^2;
skew_a= (M3_a./M0_a-3*mu_a.*var_a-mu_a.^3.)./(var_a.^(3/2));
```

Function 4

```
%Name:     num_mom_func.m

%Purpose: Sets up the ODEs for the numerical spatial moment analysis

        function du= num_mom_test(t,u,flag,a,U,b)

        du(1)=-(b/(1-a))*(u(1)-u(2));
        du(2)=(b/a)*(u(1)-u(2));

        du(3)=-(b/(1-a))*(u(3)-u(4))+(U*u(1))/(1-a);
        du(4)=(b/a)*(u(3)-u(4));

        du(5)=-(b/(1-a))*(u(5)-u(6))+(2*U*u(3))/(1-a);
        du(6)=(b/a)*(u(5)-u(6));

        du(7)=-(b/(1-a))*(u(7)-u(8))+(3*U*u(5))/(1-a);
        du(8)=(b/a)*(u(7)-u(8));

        du=du';


        end
```

Function 5

```
%Name:     num_moments.m

%Purpose: Solves the set of ODEs from num_mom_func.m with ode45


clear; close all


%this is the num

a=0.1;
U=0.1;
b=0.01;
M=1;
s=1/sqrt(pi);


tend=400;
u0=[M/(1-a),0,0,0,((s^2)*M)/(1-a),0,0,0];
[t,u]=ode45('num_mom_func',[0 tend],u0,[],a,U,b);


 M0_n=u(:,1)*(1-a)+ a*u(:,2);
 M1_n= u(:,3)*(1-a)+ a*u(:,4);
 M2_n= u(:,5)*(1-a)+ a*u(:,6);
 M3_n= u(:,7)*(1-a)+ a*u(:,8);
 mu_n= M1_n./M0_n;
 var_n= M2_n./M0_n - mu_n.^2;
 skew_n= (M3_n-3./M0_n*mu_n.*var_n-mu_n.^3.)./(var_n.^(3/2));
```

Function 6

```
%Name:     temp_moments.m

%Purpose: Solves the analytical approximations for the temporal moments

clear; close all

%Load the temporal moments computed by integrating the solution

a=0.1;
U=0.1;
b=0.01;
M=1;
s= 7.5;
C0= (M*U)/(sqrt(pi)*s*(1-a));
x=linspace(0, 100);



%Calculate the temporal moments analytically


F0t= (((1-a)*(C0*s))/U)*sqrt(pi)*(1-(1/2)*erfc(x/s));
S0t= (((1-a)*(C0*s))/U)*sqrt(pi)*(1-(1/2)*erfc(x/s));
M0t_a= (1-a)*F0t+a*S0t;

F1t=(1-a)^2*((sqrt(pi)*C0*s)/U)*(x/U);
S1t=((C0*s*sqrt(pi)*(1-a)^2)/U)*(x/U)+((C0*s*sqrt(pi))/U)*(a/b)*(1-a);
M1t_a= (1-a)^2*((sqrt(pi)*C0*s)/U)*(x/U)+(a^2/b)*(1-
a)*((C0*s*sqrt(pi))/U);




mut_a=(x/U)+a^2/b;
vart_a= 2*((a^2)/(U*b))*x+(a^3/b^2)*(2-a);
gt_a= (((6*a^3)/(U*b^2))*x+ 6*(1-a)*(a^4/b^3)+(2*a^6)/(b^3));
```

APPENDIX B: DERIVATION OF THE TEMPORAL MOMENTS

Two different solutions to the temporal moments of the Reichert and Wanner model were derived—the full solution with a Gaussian pulse initial condition and an approximate solution with a spike initial condition. The behavior of the two solutions is equal after an initial time period ($x \approx 2\sigma_0$). The expressions from the latter derivation are in a much more simplified form than the full solution so they were the only expressions presented in Chapter 3; the corresponding results from these expressions are presented in Chapter 4. Both derivations are presented in this section, however.

Full Solution

Nordin and Troutman (1980) used a relation between the Laplace transform and the moments of a distribution to compute the temporal moments for the dead zone model. If

$$\overline{C}(x,s) = L\{C(x,t)\} = \int_0^\infty e^{-st} C(x,t)dt \tag{B.1}$$

Using this relationship, the zeroth temporal moment can be written as

$$M_{0t}(x) = \int_0^\infty C(x,t)dt = \overline{C}(x,0) \tag{B.2}$$

Taking the derivative of (B.2) gives

$$\frac{\partial \overline{C}}{\partial s} = \int_0^\infty -te^{-st} C(x,t)dt \tag{B.3}$$

The nth derivative can be written as

$$\frac{\partial^n \overline{C}}{\partial s^n} = \int_0^\infty (-1)^n t^n e^{-st} C(s,t)dt \tag{B.4}$$

The nth moment can be written as

$$M_{nt}(x) = (-1)^n \left. \frac{\partial^n \overline{C}}{\partial s^n} \right|_{s=0} \tag{B.5}$$

To compute the zeroth temporal moment, the derivative is raised to the zeroth power; this

gives $\overline{C}(x,s)$ which was computed in Chapter 3. In Chapter 3, the Laplace transform of C_1

was defined as

$$\overline{C}_1(x,s) = \overline{N}(x,s') \tag{B.6}$$

where

$$s' = s + \frac{\beta}{1-\alpha}\left(1 - \frac{\beta}{\alpha s + \beta}\right) \tag{B.7}$$

and

$$N(x,t) = C_0 e^{-\frac{1}{\sigma_0^2}\left(x - \frac{\overline{U}t}{1-\alpha}\right)^2} \tag{B.8}$$

The transform of (B.8) is

$$\overline{N}(x,s) = \frac{\sqrt{\pi}}{2} C_0 \frac{\sigma_0}{U_1} erfc\left(\frac{\sigma_0 s}{2U_1} - \frac{x}{\sigma_0}\right) e^{\left(\frac{1}{4}\frac{s^2 \sigma_0^2}{U_1^2} - \frac{sx}{U_1}\right)} \tag{B.9}$$

where

$$U_1 = \frac{\overline{U}}{1-\alpha} \tag{B.10}$$

Substituting s' into (B.9) gives the transform of C_1

$$\overline{C}_1(x,s) = \overline{N}(x,s') = \frac{\sqrt{\pi}}{2} C_0 \frac{\sigma_0}{U_1} erfc\left[\frac{\sigma_0}{2U_1}\left(s + \frac{\beta}{1-\alpha} - \frac{\beta^2}{(1-\alpha)(\alpha s + \beta)} - \frac{x}{\sigma_0}\right)\right] \tag{B.11}$$

$$e^{\left[\frac{1}{4}\frac{\sigma_0^2}{U_1^2}\left(s + \frac{\beta}{1-\alpha} - \frac{\beta^2}{(1-\alpha)(\alpha s + \beta)}\right)^2 - \frac{x}{\sigma_0}\left(s + \frac{\beta}{1-\alpha} - \frac{\beta^2}{(1-\alpha)(\alpha s + \beta)}\right)\right]}$$

Setting $s = 0$, the zeroth temporal moment in the flowing zone, F_{0t}, is derived

$$F_{0t} = \overline{C}_1(x,0) = (1-\alpha)\sqrt{\pi}C_0 \frac{\sigma_0}{U}\left[1 - \frac{1}{2}erfc\left(\frac{x}{\sigma_0}\right)\right] \tag{B.12}$$

Given the definition for the transform of C_2 from Chapter 3 (Eq. 68) and setting $s = 0$, the

zeroth temporal moment in the stagnant zone is computed. It is equal to F_{0t}. The composite

zeroth moment M_{0t} is

$$M_{0t} = (1-\alpha)\sqrt{\pi}C_0 \frac{\sigma_0}{U}\left[1 - \frac{1}{2}erfc\left(\frac{x}{\sigma_0}\right)\right] \tag{B.13}$$

When $x > 2\sigma_0$

$$M_{0t} = \frac{C_0\sigma_0\sqrt{\pi}}{U}(1-\alpha) \tag{B.14}$$

Using the definition in Eq. B.5 and the procedure applied to derive the zeroth temporal

moment, the expressions for the first, second and third temporal moments are derived. The

solutions to $F_{1t}, S_{1t}, M_{1t}, F_{2t}, S_{2t}, M_{2t}, F_{3t}, S_{3t}$, and M_{3t} are

$$F_{1t} = -\frac{1}{2}\frac{(-1+\alpha)C_0\sigma_0\left(x\sqrt{\pi} + x\sqrt{\pi}erf\left(\frac{x}{\sigma_0}\right) + e^{-\frac{x^2}{\sigma_0^2}}\sigma_0\right)}{\overline{U}^2} \tag{B.15}$$

$$S_{1t} = -\frac{1}{2}\left[(-1+\alpha)C_0\sigma_0\left(x\sqrt{\pi}\beta + x\beta\sqrt{\pi}erf\left(\frac{x}{\sigma_0}\right)\right.\right.$$
$$\left.\left. + e^{-\frac{x^2}{\sigma_0^2}}\sigma_0\beta + \sqrt{\pi}\alpha\overline{U} + \sqrt{\pi}\alpha\overline{U}erf\left(\frac{x}{\sigma_0}\right)\right)\right]/\left[\overline{U}^2\beta\right] \tag{B.16}$$

$$M_{1t} = -\frac{1}{2}\left[(-1+\alpha)C_0\sigma_0\left(x\sqrt{\pi}\beta + x\beta\sqrt{\pi}erf\left(\frac{x}{\sigma_0}\right)\right.\right.$$
$$\left.\left. + e^{-\frac{x^2}{\sigma_0^2}}\sigma_0\beta + \sqrt{\pi}\alpha^2\overline{U} + \sqrt{\pi}\alpha^2\overline{U}erf\left(\frac{x}{\sigma_0}\right)\right)\right]/\left[\overline{U}^2\beta\right]$$

(B.17)

$$F_{2t} = -\frac{1}{4}\frac{1}{\overline{U}^3\beta}\left[(-1+\alpha)C_0\sigma_0\left(4\sqrt{\pi}\,\alpha^2 x\overline{U} + 4\sqrt{\pi}\alpha^2 x\overline{U}erf\left(\frac{x}{\sigma_0}\right)\right.\right.$$
$$+\sqrt{\pi}\alpha^2\beta + \sqrt{\pi}\alpha^2\beta erf\left(\frac{x}{\sigma_0}\right) + 2x^2\sqrt{\pi}\beta + 2x^2\sqrt{\pi}\beta erf\left(\frac{x}{\sigma_0}\right)$$
$$\left.\left. + 2xe^{-\frac{x^2}{\sigma_0^2}}\sigma_0\beta + 4e^{-\frac{x^2}{\sigma_0^2}}\alpha^2\sigma_0\overline{U}\right)\right]$$

(B.18)

$$S_{2t} = -\frac{1}{4}\frac{1}{\overline{U}^3\beta^2}\left[(-1+\alpha)C_0\sigma_0\left(4\sqrt{\pi}\,\alpha^2 x\overline{U} + 4\sqrt{\pi}\beta\alpha^2 x\overline{U}erf\left(\frac{x}{\sigma_0}\right)\right.\right.$$
$$+\sqrt{\pi}\sigma_0^2\beta^2 + \sqrt{\pi}\sigma_0^2\beta erf\left(\frac{x}{\sigma_0}\right) + 2x^2\sqrt{\pi}\beta^2 + 2x^2\sqrt{\pi}\beta^2 erf\left(\frac{x}{\sigma_0}\right)$$
$$+2xe^{-\frac{x^2}{\sigma_0^2}}\sigma_0\beta^2 + 4x\sqrt{\pi}\alpha\overline{U}\beta + 4x\sqrt{\pi}\alpha\overline{U}\beta erf\left(\frac{x}{\sigma_0}\right)$$
$$\left.\left. + 4e^{-\frac{x^2}{\sigma_0^2}}\alpha^2\sigma_0\overline{U}\beta + 4e^{-\frac{x^2}{\sigma_0^2}}\alpha\sigma_0\overline{U}\beta + 4\sqrt{\pi}\alpha^2\overline{U}^2 + 4\sqrt{\pi}\alpha^2\overline{U}^2 erf\left(\frac{x}{\sigma_0}\right)\right)\right]$$

(B.19)

$$M_{2t} = -\frac{1}{4}\frac{1}{\overline{U}^3\beta^2}\left[(-1+\alpha)C_0\sigma_0\left(8\sqrt{\pi}\,\beta\alpha^2 x\overline{U} + 8\sqrt{\pi}\beta\alpha^2 x\overline{U}erf\left(\frac{x}{\sigma_0}\right)\right.\right.$$
$$+\sqrt{\pi}\sigma_0^2\beta^2 + 4\sqrt{\pi}\alpha^3\overline{U}^2 + \sqrt{\pi}\sigma_0^2\beta^2 erf\left(\frac{x}{\sigma_0}\right) + 2x^2\sqrt{\pi}\beta^2$$
$$+2x^2\sqrt{\pi}\beta^2 erf\left(\frac{x}{\sigma_0}\right) + 2xe^{-\frac{x^2}{\sigma_0^2}}\sigma_0\beta^2$$
$$\left.\left. + 8e^{-\frac{x^2}{\sigma_0^2}}\alpha^2\sigma_0\overline{U}\beta + 4\sqrt{\pi}\alpha^3\overline{U}^2 erf\left(\frac{x}{\sigma_0}\right)\right)\right]$$

(B.20)

$$F_{3t} = -\frac{1}{4}\frac{1}{\beta^2 U^4}\Big[C_0\sigma_0\left(-1+\alpha\right)\Big(12\alpha^3\sqrt{\pi}\,\overline{U}^2 x$$

$$+12\alpha^3\sqrt{\pi}\,\overline{U}^2 x\,erf\left(\frac{x}{\sigma_0}\right) + 6\alpha^2\sqrt{\pi}\,\overline{U}\sigma_0^2\beta + 6\alpha^2\sqrt{\pi}\,\overline{U}\sigma_0^2\beta\,erf\left(\frac{x}{\sigma_0}\right)$$

$$+12x^2\sqrt{\pi}\,\beta\alpha^2\overline{U} + 12x^2\sqrt{\pi}\,\beta\alpha^2\overline{U}erf\left(\frac{x}{\sigma_0}\right) + 3x\sqrt{\pi}\,\beta^2\sigma_0^2$$

$$+3x\sqrt{\pi}\,\beta^2\sigma_0^2 erf\left(\frac{x}{\sigma_0}\right) + 12e^{-\frac{x^2}{\sigma_0^2}}\sigma_0\beta\alpha^2 x\overline{U} + 2\sigma_0^2 e^{-\frac{x^2}{\sigma_0^2}}\beta^2$$

$$+2x^3\sqrt{\pi}\,\beta^2 + 2x^3\sqrt{\pi}\,\beta^2 erf\left(\frac{x}{\sigma_0}\right) + 2x^2 e^{-\frac{x^2}{\sigma_0^2}}\sigma_0\beta^2 + 12e^{-\frac{x^2}{\sigma_0^2}}\alpha^3\overline{U}^2\Big)\Big] \tag{B.21}$$

$$S_{3t} = -\frac{1}{4}\frac{1}{\beta^2 U^4}\Big[C_0\sigma_0\left(-1+\alpha\right)\Big(2\beta^3\sqrt{\pi}\,x^3$$

$$+12\alpha^3\sqrt{\pi}\,\overline{U}^3 erf\left(\frac{x}{\sigma_0}\right) + 12\alpha^3\sqrt{\pi}\,\overline{U}^3 + 12e^{-\frac{x^2}{\sigma_0^2}}\alpha^2\overline{U}^2\sigma_0\beta$$

$$+2x^2 e^{-\frac{x^2}{\sigma_0^2}}\sigma_0\beta^3 + 6xe^{-\frac{x^2}{\sigma_0^2}}\sigma_0\beta^2\alpha\overline{U} + 2x^3\sqrt{\pi}\,\beta^3 erf\left(\frac{x}{\sigma_0}\right)$$

$$+2\sigma_0^3 e^{-\frac{x^2}{\sigma_0^2}}\beta^3 + 24e^{-\frac{x^2}{\sigma_0^2}}\sigma_0\alpha^3\beta\overline{U}^2 + 12e^{-\frac{x^2}{\sigma_0^2}}\sigma_0\beta^2\alpha^2 x\overline{U} + 6x^2\sqrt{\pi}\,\alpha\beta^2\overline{U}$$

$$+6x^2\sqrt{\pi}\,\alpha\beta^2\overline{U}erf\left(\frac{x}{\sigma_0}\right) + 24\alpha^3\sqrt{\pi}\,\beta\overline{U}^2 x + 24\alpha^3\sqrt{\pi}\,\beta\overline{U}^2 x\,erf\left(\frac{x}{\sigma_0}\right)$$

$$+6\alpha^2\sqrt{\pi}\,\beta^2\overline{U}\sigma_0^2 + 6\alpha^2\sqrt{\pi}\,\beta^2\overline{U}\sigma_0^2 erf\left(\frac{x}{\sigma_0}\right) + 3\sqrt{\pi}\,\alpha\beta^2\overline{U}\sigma_0^2$$

$$+3\sqrt{\pi}\,\alpha\beta^2\overline{U}\sigma_0^2 erf\left(\frac{x}{\sigma_0}\right) + 12x^2\sqrt{\pi}\,\beta^2\alpha^2\overline{U}erf\left(\frac{x}{\sigma_0}\right)$$

$$+3x\sqrt{\pi}\,\beta^3\sigma_0^2 erf\left(\frac{x}{\sigma_0}\right)$$

$$+12x\sqrt{\pi}\,\alpha^2\beta\overline{U}^2 + 12x\sqrt{\pi}\,\alpha^2\beta\overline{U}^2 erf\left(\frac{x}{\sigma_0}\right) + 3x\sqrt{\pi}\,\beta^3\overline{U}^2\Big)\Big] \tag{B.22}$$

$$M_{3t} = -\frac{1}{4}\frac{1}{\beta^2 U^4}\Big[C_0\sigma_0(-1+\alpha)(18x^2\sqrt{\pi}\beta^2\alpha^2\overline{U}$$

$$+3x\sqrt{\pi}\beta^3\sigma_0^2 + 18x^2\alpha^2\sqrt{\pi}\beta^2\overline{U}erf\left(\frac{x}{\sigma_0}\right) + 2x^2 e^{-\frac{x^2}{\sigma_0^2}}\sigma_0\beta^3$$

$$+3x\sqrt{\pi}\beta^3\sigma_0^2 erf\left(\frac{x}{\sigma_0}\right) + 2x^3\sqrt{\pi}\beta^3 + 2\sigma_0^3 e^{-\frac{x^2}{\sigma_0^2}}\beta^3 + 12\sqrt{\pi}\alpha^4\overline{U}^3$$

$$+18\sigma e^{-\frac{x^2}{\sigma_0^2}}\beta^2\alpha^2 x\overline{U} + 24 e^{-\frac{x^2}{\sigma_0^2}}\sigma_0\alpha^3\beta\overline{U}^2 + 24\alpha^3\sqrt{\pi}\beta\overline{U}^2 x$$

$$+12\sqrt{\pi}\alpha^4\overline{U}^2 erf\left(\frac{x}{\sigma_0}\right) + 2x^3\sqrt{\pi}\beta^3 erf\left(\frac{x}{\sigma_0}\right)$$

$$+12\beta\alpha^4\sqrt{\pi}\overline{U}^2 x + 24\alpha^3\sqrt{\pi}\beta\overline{U}^2 xerf\left(\frac{x}{\sigma_0}\right)$$

$$+9\alpha^2\sqrt{\pi}\beta^2\overline{U}\sigma_0^2 + 9\alpha^2\sqrt{\pi}\beta^2\overline{U}\sigma_0^2 erf\left(\frac{x}{\sigma_0}\right)$$

$$+12\sqrt{\pi}\alpha^4\beta\overline{U}^2 xerf\left(\frac{x}{\sigma_0}\right) + 12\beta e^{-\frac{x^2}{\sigma_0^2}}\sigma_0\alpha^4\overline{U}^2\Big)\Big]$$

(B.23)

Approximate Solution

When the initial input is in the form of a spike, instead of a Gaussian pulse, (B.11)

becomes

$$\overline{N}(x,s') = \frac{M(1-\alpha)}{\overline{U}} e^{-\frac{s'x}{\overline{U}}(1-\alpha)}$$

(B.24)

The same procedure used to derive the full solution is used to derive the expressions for the

approximate solution. The approximate solutions to $F_{0t}, S_{0t}, F_{1t}, S_{1t}, M_{1t}, F_{2t}, S_{2t}, M_{2t}, F_{3t}, S_{3t},$

and M_{3t} are

$$F_{0t} = S_{0t} = M_{0t} = M\frac{(1-\alpha)}{\overline{\overline{U}}} \tag{B.25}$$

$$F_{1t} = \frac{M(1-\alpha)}{\overline{\overline{U}}}\frac{x}{\overline{\overline{U}}} \tag{B.26}$$

$$S_{1t} = \frac{M(1-\alpha)}{\overline{\overline{U}}}\frac{x}{\overline{\overline{U}}}\left(1+\frac{\alpha\overline{U}}{\beta x}\right) \tag{B.27}$$

$$M_{1t} = \frac{M(1-\alpha)}{\overline{\overline{U}}}\frac{x}{\overline{\overline{U}}}\left(1+\frac{\alpha^2\overline{U}}{\beta x}\right) \tag{B.28}$$

$$F_{2t} = \frac{M(1-\alpha)}{\overline{\overline{U}}}\frac{x}{\overline{\overline{U}}^2\beta}\left(2\alpha^2\overline{U}+x\beta\right) \tag{B.29}$$

$$S_{2t} = \frac{M(1-\alpha)}{\overline{U}^3\beta^2}\left(2\alpha^2 x\overline{U}\beta+x^2\beta^2+2\alpha^2\overline{U}^2\right) \tag{B.30}$$

$$M_{2t} = \frac{M(1-\alpha)}{\overline{U}^3\beta^2}\left(4\alpha^2 x\overline{U}\beta+x^2\beta^2+2\alpha^3\overline{U}^2\right) \tag{B.31}$$

$$F_{3t} = \frac{M(1-\alpha)x}{\overline{U}^4\beta^2}\left(6\alpha^3\overline{U}^2+6\alpha^2 x\overline{U}\beta+x^2\beta^2\right) \tag{B.32}$$

$$\begin{aligned} S_{3t} = \frac{M(1-\alpha)}{\overline{U}^4\beta^3}\Big(&12\alpha^3 x\overline{U}^2\beta+6\alpha^2 x^2\overline{U}\beta^2+x^3\beta^3 \\ &+3x^2\alpha\overline{U}\beta^2+6x\alpha^2\overline{U}^2\beta+6\alpha^3\overline{U}^3\Big) \end{aligned} \tag{B.33}$$

$$\begin{aligned} M_{3t} = \frac{M(1-\alpha)}{\overline{U}^4\beta^3}\Big(&12\alpha^3 x\overline{U}^2\beta+9\alpha^2 x^2\overline{U}\beta^2+x^3\beta^3 \\ &+6x\alpha^4\overline{U}^2\beta+6\alpha^4\overline{U}^3\Big) \end{aligned} \tag{B.24}$$

These expressions are used to create Eq. 105-108.

REFERENCES

Akhtar, W. 1978. Study of mixing in natural streams and air agitated tanks. Windsor, Ontario, Canada: University of Windsor.

Aris, R. (1956) On the dispersion of a solute in a fluid flowing through a tube. *Proceedings of the Royal Society of London Series A-Mathematical and Physical Sciences,* 235**,** 67-77.

Bencala, K. E. & R. A. Walters (1983) Simulation of solute transport in a mountain pool-and-riffle stream - a transient storage model. *Water Resources Research,* 19**,** 718-724.

Carr, M. L. & C. R. Rehmann (2007) Measuring the dispersion coefficent with acoustic Doppler current profilers. *Journal of Hydraulic Engineering,* 133**,** 977-982.

Chang, Y. C. 1971. Lateral mixing in meandering streams. *PhD Thesis*, University of Iowa.

Chatwin, P. C. (1972) Cumulants of distribution of concentration of a solute dispersing in solvent flowing through a tube. *Journal of Fluid Mechanics,* 51**,** 63.

Davis, P. M., T. C. Atkinson & T. M. L. Wigley (2000) Longitudinal dispersion in natural channels: 2. The roles of shear flow dispersion and dead zones in the River Severn, UK. *Hydrology and Earth System Sciences,* 4**,** 355-371.

Day, T. J. (1975) Longitudinal dispersion in natural channels. *Water Resources Research,* 11**,** 909-918.

Day, T. J. & I. R. Wood (1976) Similarity of mean motion of fluid particles dispersing in a natural channel. *Water Resources Research,* 12**,** 655-666.

De Smedt, F. (2006) Analytical solutions for transport of decaying solutes in rivers with transient storage. *Journal of Hydrology,* 330**,** 672-680.

De Smedt, F., W. Brevis & P. Debels (2005) Analytical solution for solute transport resulting from instantaneous injection in streams with transient storage. *Journal of Hydrology,* 315**,** 25-39.

Denton, R. A. (1990) Analytical asymptotic solutions for longitudinal dispersion with dead zones. *Journal of Hydraulic Research,* 28**,** 309-329.

Elder, J. W. (1959) The dispersion of marked fluid in turbulent shear flow. *Journal of Fluid Mechanics,* 5**,** 544-560.

Fischer, H. B. (1966). Longitudinal dispersion in laboratory and natural streams, *Rep, No. KH-R-12*, California Institute of Technology, Pasadena.

Fischer, H. B. (1967) The mechanics of dispersion in natural streams. *Journal of the Hydraulics Division-ASCE,* 93 (HY6)**,** 187-215.

Fischer, H. B. (1968) Dispersion predictions in natural streams. *Journal of the Hydraulics Division-ASCE,* SA5**,** 927-943.

Fishcher, H.B. (1973) Longitudinal dispersion and turbulent mixing in open-channel flow. *Annual Review of Fluid Mechanics,* 5**,** 59-78.

Fischer, H.B. (1975) Simple method for predicting dispersion in streams. *Journal of the Environmental Engineering Division-ASCE,* 101**,** 453-455.

Fischer, H. B., E. J. List, R. C. Y. Koh, J. Imberger & N. H. Brooks. 1979. *Mixing in Inland and Coastal Waters*. New York: Academic Press, Inc.

Gowda, T. P. H. (1984) Water-quality prediction in mixing zones of rivers. *Journal of Environmental Engineering,* 110**,** 751-769.

Harden, T. O. & H. T. Shen (1979) Numerical-simulation of mixing in natural rivers. *Journal of the Hydraulics Division-ASCE,* 105**,** 393-408.

Hays, J. R. 1966. Mass transport phenomena in open channel flow. *PhD Thesis*, Vanderbilt University, Nashville.

Holley, E. R. & G. H. Jirka. 1986. Mixing in Rivers. Vicksburg, MS: U.S. Army Engineers Water Experimental Station.

Holly, F. M. 1975. Two-dimensional mass dispersion in rivers. In *Hydrol. Pap 78*. Fort Collins: Colorado State University.

Hunt, B. (1999) Dispersion model for mountain streams. *Journal of Hydraulic Engineering,* 125**,** 99-105.

Jobson, H. E. (1997) Predicting travel time and dispersion in rivers and streams. *Journal of Hydraulic Engineering,* 123**,** 971-978.

Kadlec, R. H. (1994) Detention and mixing in free-water wetlands. *Ecological Engineering,* 3**,** 345-380.

Lau, Y. L. & B. G. Krishnappan (1981) Modeling transverse mixing in natural streams. *Journal of the Hydraulics Division-ASCE,* 107**,** 209-226.

Legrandmarcq, C. & H. Laudelout (1985) Longitudinal dispersion in a forest stream. *Journal of Hydrology,* 78**,** 317-324.

Liu, H. & H. D. Cheng (1980) Modified Fickian model for predicting dispersion. *Journal of the Hydraulics Division-ASCE,* 106 (HY6)**,** 1021-1040.

Luk, G. K. Y., Y. L. Lau & W. E. Watt (1990) 2-dimensional mixing in rivers with unsteady pollutant source. *Journal of Environmental Engineering,* 116**,** 125-143.

Mathworks. "Product Documentation." *R2012a Documentation: MATLAB*. Mathworks, 2012. Web. 15 Apr. 201. <http://www.mathworks.com/help/techdoc/ref/ode23.html>.

MATLAB version R2012a. Natick, Massachusetts: The MathWorks Inc., 2012

McCorquodale, J. A. (1983) Transport of pollutants in natural streams. *Canadian Journal of Civil Engineering,* 10 (1)**,** 9-17.

Nordin, C.F., Jr., and Sabol, G.V., 1974, Empirical data on longitudinal dispersion in rivers: U.S. Geological Survey. *Water-Resources Investigations* 332, 20-74.

Nordin, C. F. & B. M. Troutman (1980) Longitudinal dispersion in rivers - the persistence of skewness in observed data. *Water Resources Research,* 16**,** 123-128.

Onishi, Y. & M. Asce (1981) Sediment-contaminant transport model. *Journal of the Hydraulics Division-ASCE,* 107**,** 1089-1107.

Reichert, P. & O. Wanner (1991) Enhanced one-dimensional modeling of transport in rivers. *Journal of Hydraulic Engineering,* 117**,** 1165-1183.

Runkel, R. L. & S. C. Chapra (1993) An efficient numerical-solution of the transient storage equations for solute transport in small streams. *Water Resources Research,* 29**,** 211-215.

Runkel, Rob. "One-Dimensional Transport with Inflow and Storage (OTIS): A Solute Transport Model for Streams and Rivers." *OTIS*. USGS, 17 Aug. 2011. Web. 15 Apr. 2012. <http://water.usgs.gov/software/OTIS/>.

Rutherford, J. C. 1994. *River Mixing*. Baffin Lane, Chichester, West Sussex PO19 1UD, England: John Wiley & Sons.

Sayre, W. W. 1968. Dispersion of mass in open channel flow. *PhD Thesis*, Colorado State University, Fort Collins.

Sayre, W.W., Chang, F.M., 1968. A Laboratory Investigation of the Open Channel Dispersion Process of Dissolved, Suspended and Floating Dispersants. US Geological Survey, Professional Paper 433-E.

Schmid, B. H. (2002) Persistence of skewness in longitudinal dispersion data: Can the dead zone model explain it after all? *Journal of Hydraulic Engineering,* 128**,** 848-854.

Seo, I. W. & T. S. Cheong (1998) Predicting longitudinal dispersion coefficient in natural streams. *Journal of Hydraulic Engineering,* 124**,** 25-32.

Seo, I. W. & T. S. Cheong (2001) Moment-based calculation of parameters for the storage zone model for river dispersion. *Journal of Hydraulic Engineering,* 127**,** 453-465.

Sneddon, I. H. 1972. *The Use of Integral Transforms*. McGraw-Hill Book Company.

Somlyody, L. (1982) An approach to the study of transverse mixing in streams. *Journal of Hydraulic Research,* 20**,** 203-220.

Taylor, G. (1953). Dispersion of soluble matter in solvent flowing slowly through a tube. *Proceedings of the Royal Society of London Series A-Mathematical and Physical Sciences,* 219**,** 186-203.

Taylor, G. (1954) The dispersion of matter in turbulent flow through a pipe. *Proceedings of the Royal Society of London Series A-Mathematical and Physical Sciences,* 223**,** 446-468

Tsai, Y. H. & E. R. Holley (1978) Temporal moments for longitudinal dispersion. *Journal of the Hydraulics Division-ASCE,* 104**,** 1617-1634.

Valentine, E. M. & I. R. Wood (1977) Longitudinal dispersion with dead zones. *Journal of the Hydraulics Division-ASCE,* 103**,** 975-990.

Valentine, E. M. (1978). The effects of channel boundary roughness on longitudinal dispersion. *PhD Thesis*, University of Cantebury, Christchurch.

Valentine and Wood (1979) Experiments in longitudinal dispersion with dead zones. *Journal of the Hydraulics Division-ASCE,* 105**,** 999-1016

Verboom, G. K. 1974. Transverse mixing in rivers; a numerical approach. *Report 117, Delft Hydr. Lab.*, Delft, The Netherlands.

Yotsukura, N. & W. W. Sayre (1976) Transverse mixing in natural channels. *Water Resources Research,* 12**,** 695-704.